Planning integrated energy systems coupling V2G as a flexible storage

Hongqian Wei [a,b], Youtong Zhang [a], Yongzhen Wang [c], Weiqi Hua [b], Rui Jing [b,*], Yue Zhou [b,*].

a School of Mechanical Engineering, Beijing Institute of Technology, Beijing, 100081, China

b School of Engineering, Cardiff University, Cardiff CF24 3AA, UK

c Department of Electrical Engineering, Energy Internet Research Institute, Tsinghua University, Beijing 100084, China

Abstract

Coupling the vehicle-to-grid (V2G) with integrated energy systems (IES) offers an emerging solution for decarbonisation of both energy and transport sectors. To evaluate the feasibility of coupling V2G with IES as a flexible storage, we propose an optimisation-based system planning framework embedding V2G into IES. Within this framework, stochastic features of electric vehicles (EV) fleets are simulated. The impacts of V2G on IES design are captured by assessing both economic and environmental benefits via multi-objective optimisations utilising an improved NSGA-II algorithm. Six case studies considering three cities with different climate conditions and two functional areas of residential and commercial are performed. The results manifest that Beijing-commercial case could achieve the largest mutual benefits. The EV fleets' charging behaviour follows the time-of-use energy tariff in transition seasons while not during winter. Sensitivity analysis indicates the electricity and gas prices have significant impact on the system design. The benefits induced by growing EV penetration would gradually decrease and stabilize when the EV number reach 300, the growth of economic and environmental benefits stabilized at 1.3% and 1.8%, respectively. Overall, this study quantifies the benefits of enabling V2G in IES, and generates valuable insights for IES planners, V2G service providers, and relevant policymakers.

Keywords: integrated energy system; vehicle to grid; electric vehicles; flexible energy storage; multi-objective optimisation; feasibility assessment.

---

*Corresponding author.

✉E-mail: Jingr2@cardiff.ac.uk (R.J.) ZhouY68@cardiff.ac.uk (Y.Z.)

1 Introduction

Excessive consumption of fossil fuels and the resulting greenhouse effect have touched everyone's nerve globally. Decarbonisation requires joint efforts from all nations or regions. EU is managing to cut the total industrial CO_2 emission by 40% before 2030 compared with the levels in the 1990s. [1]. China, the nation covering 1/7 of global CO_2 emissions, has committed to reach the "carbon neutrality" before 2060 [2]. Driven by the governmental policies, the advanced approaches in the multiple energy system, e.g., increasing renewable energy share, and coupling the energy with other sectors, e.g. the transport sector, has been regarded as a promising way for global decarbonisation [3-5].

1.1 Relevant research

In recent years, research efforts have been made on designing the integrated energy systems (IES) that fulfils electrical, heating, and cooling demands simultaneously. Current research has covered the multi-objective optimisation from economic and carbon emission perspectives [6], planning [7] and scheduling [8], handling uncertainty [9], and evaluating reliability and resilience [10]. The demand response has been reviewed in [11], in which the generation expansion planning problem is significantly analysed and points that EV integration would be the future challenge. Rabiee et al. [12] constructed the stochastic multi-objective optimisation model to evaluate the trade-off between the system cost and environmental issues. Yang et al. [13] established a set of interconnected energy hubs to enhance the flexibility and reliability of the IES, in which the cost of purchasing energy and revenue from the feed-in tariff are critically considered. Wang et al. [14] adopted the Monte Carlo simulation to capture uncertainties from multiple parameters when designing a building-based IES. The uncertainties' impact on system economic and emissions performances are analysed. To quantify the flexibility of IES considering the dynamic uncertainty, Qin et al. developed the generalised quasi-dynamics model and decomposition-iteration methods for optimal scheduling of the electric-heat coupling IES [15]. Perera et al. [16] developed the extreme weather model and quantified the climate uncertainty's impact on the urban energy systems by calculating the associated energy infrastructure cost. Lv et al. [17] proposed and optimised an energy-water nexus system to reduce the water utilisation

but compensate the local coal-fired power-generation shortage. Wang et al. [18] proposed the cost-effective and environmental-friendly power supply chain to analyse its self-sufficiency probability and optimise the energy balance with high penetration of renewable. Pfeifer et al. [19] has investigated the flexibility and economic cost of the EnergyPLAN model which modelled the renewable energy sources, storage technologies and demand response. In this study, through introducing the flexibility, the annual cost of the energy system has been reduced due to the decreasing installed capacity. Jin et al. investigated the potential and operation strategy of microgrids enabling demand response [20] with optimised dynamic pricing strategy. Jing et al. [21] developed the urban rooftop food-energy-nexus system which offered a promising solution to the reduce carbon emission with limited urban land-use. In general, applying the systemic thinking by coupling energy systems with other sectors could offer mutual benefits to mitigate greenhouse gas emissions and call for more research efforts.

Vehicle to grid (V2G) technology could potentially offer various services, including the voltage and frequency regulation [22, 23], balancing intermittent renewables [24], and generating economic and environmental benefits [25]. Preliminary attempts have made to enable EVs as the power storage technology in the IES. Zhang et al. [26] investigated the EV load increase in the future 20 years, and quantified the benefits of optimised EV charge on the load flexibility. Jing et al. [27] modelled the supply chain profit-allocation of retired batteries and designed the fair profit distribution with the game-theory based optimisation. Prebeg et al. [28] have balanced the fuel cost and the energy trade with consideration of EV batteries in the two-level long-term multi-objective optimisation of the Croatian energy system. Tran et al. [29] discussed the battery charging type and concluded that the different charging ratios have an important effect on the real-world V2G applications. Duan et al. [30] investigated the cooling energy for the battery utilization, in which the depth of discharge has been significantly analysed in consideration of the energy consumption. Shi et al. [31] employed V2G technologies to stabilise the intermittency of renewable energy sources, in which the uncertainties of wind energy and EV charging states were modelled with the robust worst-case strategy. To fully explore the V2G accessibility in the IES system, Fathabadi et al. [32] featured the EV and plug-in hybrid EVs (PHEVs) fleets combining with the distributed generators. Sedighizadeh et al. [33] integrated the PHEV and the battery energy storage (BES)

into the microgrid for the sustainable energy solution. Results manifested that compared with the BES, PHEVs possessed a considerable potential in managing energy consumption and emissions. Akhoundzadeh et al. [34] integrated the lithium-ion battery and hydrogen fuel cell in the EVs to explore the energy utilization and analysed the system response for the power split progress. Besides, Panchal et al. investigated the degradation testing for a lithium-ion battery and estimated the battery life under different discharge conditions. Wolinetz et al. [35] simulated the impact of consumer behaviour on V2G benefits, and found that the adoption of EVs would not increase but electricity prices would be reduced by 0.6~0.7% by 2050 compared with the scenarios without V2G. For more practicalities and flexibilities, EV operating pattern and battery potential, i.e. V2G availability and actual power constraints have been further considered. For instance, the dynamic charging pattern to optimise the grid demand response is performed in [36]. Zhou et al. [37] developed a robust energy dispatching strategy to address the multi-random V2G problem, in which the total peak load and operating cost were simultaneously optimised. Mu et al. [38] utilised the Monte Carlo simulation to stimulate the EV charging load and evaluate the EV penetration level in the spatial-temporal based power system. Lin et al. [39] considered the penetration rate and the charging patterns of EVs in the IES. On this basis, the EV fleets were utilised to shift the electrical load in the valley period. In [40], the EV travel time and charging probability were considered. The coordination of the V2G activities in the IES scheduling strategy was handled by the aggregator agent. All above research indicated that coupling V2G with energy systems could generate various benefits by optimal scheduling of EV and energy systems.

1.2 Knowledge gap and contribution

Within the context of IES, few studies have focused on evaluating the role of emerging V2G as a flexible and mobile storage technology. Challenges remain to capture the considerable variabilities of EV charging patterns. Therefore, **a knowledge gap exists** in comprehensively evaluating the feasibility and implications of embedding V2G into IES considering the EV's random charging behaviour and the possible system design trade-off between economic and environmental objectives. Beyond existing works aiming for the IES dispatch along with EV scheduling, this study further evaluates the impact of V2G on both IES design and dispatch simultaneously. Besides, the multi-objective and nonlinear model is

developed to capture various EV charging patterns and random charging behaviour, and further solved by an improved NSGA-II with the embedded diversity maximization algorithm. A set of case studies in three climate zones and two functional areas are then performed to unlock the value of embedding V2G into IES and identify the most suitable demonstrations considering multiple uncertainties from energy prices and the EV penetration. Compared to previous studies, two contributions of this work lie in:

(1) This study couples the energy sector and transport sector by embedding the V2G technologies into the IES, and further quantifies the impact of V2G as a mobile and flexible storage on the IES design and operation from both economic and environmental perspectives.

(2) By developing a set of cases considering three locations with different climate conditions, two functional areas and stochastic EV charging patterns, the best application for embedding V2G into IES is identified considering multiple parametric uncertainties from energy prices and EV penetration rate.

The rest of the paper is organised as follows. Section 2 introduces the V2G-IES optimisation framework and describes the model development, model solving, and decision-making approaches. The case study setup is illustrated in Section 3, and Section 4 discusses the results which is followed by the conclusion and future research outlined in Section 5.

2 Method

The outline of the proposed V2G-IES optimisation framework is illustrated in **Fig. 1**, in which the EV batteries can bidirectionally charge and discharge electricity from/to the grid. The V2G-IES fulfils basic EV charging demand, and in the meantime, the flexibility by timely scheduling EV battery could benefit the IES. The whole study includes six major steps. **Fig. 1** (a) illustrates the system layout involving the EV fleets and a typical IES that can fulfil the basic electrical, heating, and cooling demands, simultaneously. **Fig. 1** (b) refers to the parametric database including the energy system design and EV charging related data. The optimisation model formulation, multi-objective model solving, and the posterior decision-making on the obtained Pareto frontiers are illustrated by **Fig. 1** (c)~(e) considering possible system design trade-off between cost and emissions objectives. We then develop a comprehensive case study to evaluate the V2G-IES performance in six cases with three cities

(Beijing, Shanghai, Xiamen) with different climate conditions and two functional areas (i.e., commercial and residential areas) with different demand patterns. The impact of V2G on IES regarding to IES design and operation, as well as the EV charging behaviour, has been analysed considering uncertainties from energy prices and EV penetration rate as illustrated in **Fig. 1** (f).

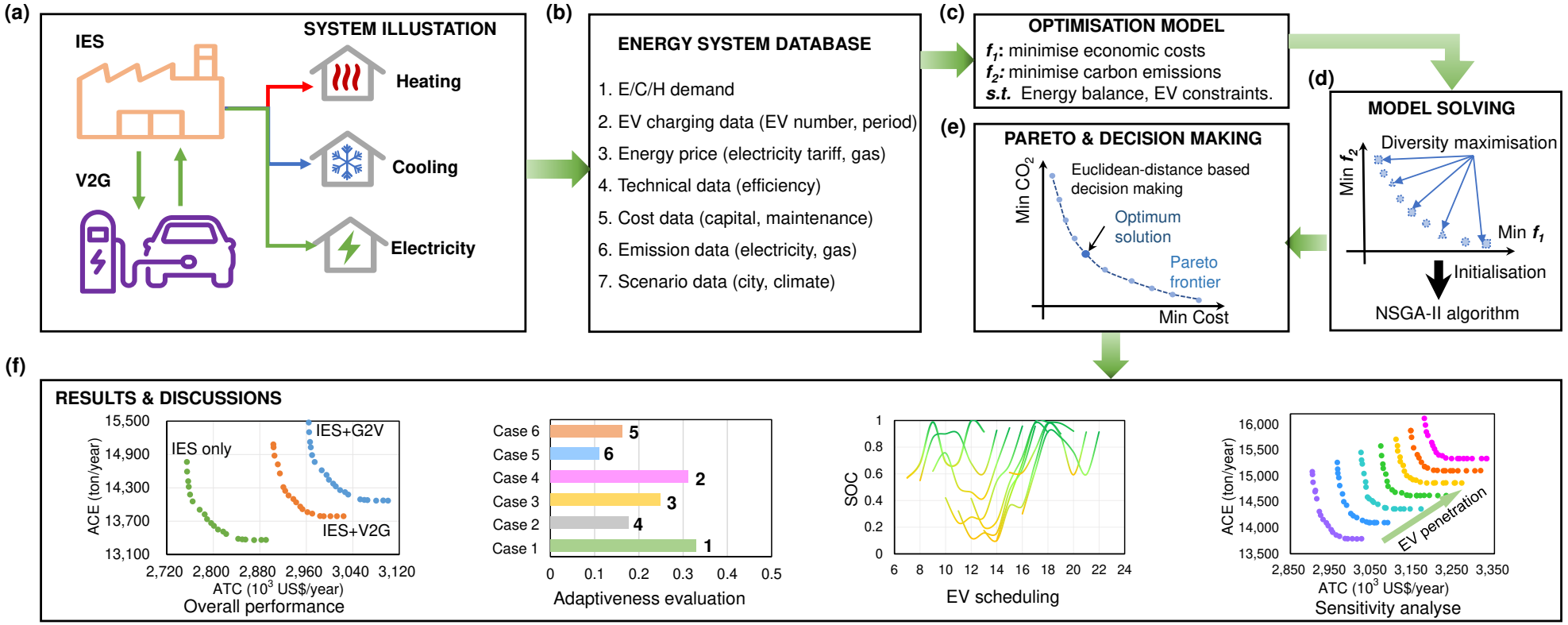

Fig. 1 Outline of the proposed optimisation framework for the V2G-IES. (a) System layout for IES integrated with EV fleets, (b) Input database related to IES and V2G, (c) Two objectives to minimise the costs and carbon emissions, respectively, (d) Model solving method by NSGA-II further developed with diversity maximization initialisation heuristic, (e) V2G-IES design trade-off represented as Pareto frontier and the Euclidean-distance based decision making method to identify one overall best solution, (f) Case study results related to the V2G-IES performance and EV charging behaviour considering uncertainties.

Note: Pareto frontier denotes a series of solutions in the situation where no individual or preference criterion can be better off without making at least on individual or preference criterion worse off or without any loss thereof. It denotes the trade-off relationship between two objectives.

2.1 V2G-IES system description

Fig. 2 illustrates the typical IES coupled with a charging station for EV fleets in which the EV fleets are enabled to interact with the IES by charging or discharging the batteries during the specified time. The IES is equipped with both renewable and conventional technologies; and the technical configuration, installed capacity, and hourly operational strategy can be optimised. In an IES, electrical, cooling and heating demands are fulfilled by the combination of multiple technologies, among which the cooling demand is satisfied by the electrical chiller and absorption chiller. Meanwhile, the IES can interact with the grid and EV fleets. By utilising the adjustable EV charging schedule, interactions via V2G, and time-of-use

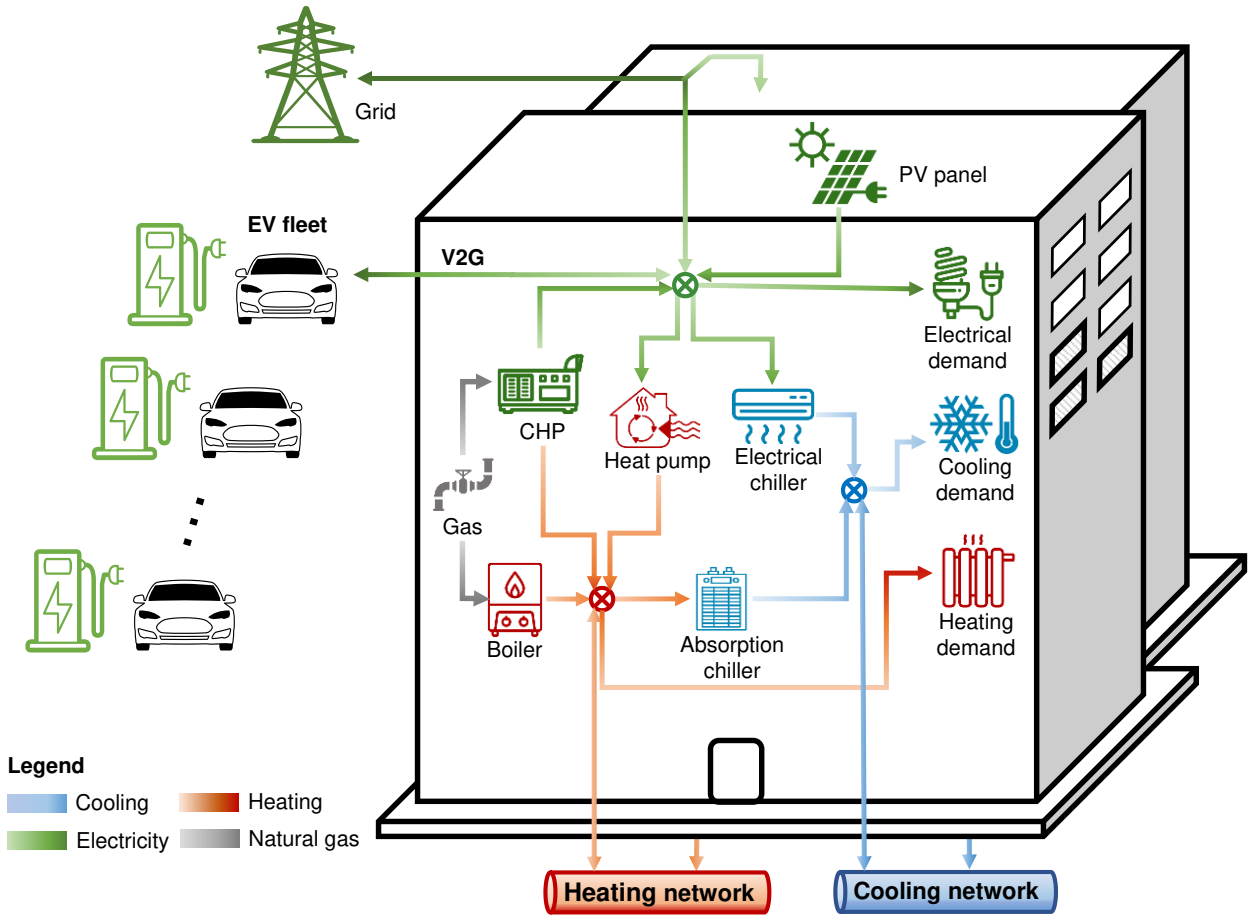

Fig. 2 Outline of the V2G-IES.

CHP is combined heating and power, PV is photovoltaic.

electricity tariff, the EV fleets with V2G functions could act as a flexible energy storage to generate the cost saving and low-carbon benefits for the whole V2G-IES.

2.2 V2G-IES model development

In the V2G-IES model, two objectives have been considered, i.e., the minimisation of annualised total cost (ATC) and the minimisation of annualised carbon emissions (ACE).

The multi-objective optimisation model can be expressed as to minimise the ATC and ACE objectives.

Min obj1 = annualised total cost (ATC) by Eqn. (1)~(3)

Min obj2 = annualised carbon emissions (ACE) by Eqn. (4)

s.t. Energy balance constraints by Eqn. (A1)~(A3)

Energy conversion constraints by Eqn. (A4)

CHP operational constraints by Eqn. (A5)~(A7)

Grid operational constraints by Eqn. (A8)

EV charging constraints by Eqn. (A9)

The ATC objective is defined in Eqn. (1), which accounts for the capital cost (*CAPEX*) and the operational cost (*OPEX*).

$$ATC = CAPEX + OPEX \tag{1}$$

The *CAPEX* contains the installation cost of energy technologies including the CHP, boiler, heat pump, absorption chiller, electric chiller, photovoltage panel as well as V2G facilities, see the definition in Eqn. (2a). The *CAPEX* is annualised with the capital recovery factor (*CRF*) in Eqn. (2b). The service life of the energy technology is assumed as 15 year.

$$CAPEX = \sum_{s} CAP_s \times UC_s^{cap} \times CRF \tag{2a}$$

$$CRF = \frac{r \times (1+r)^p}{(1+r)^p - 1} \tag{2b}$$

where CAP_s represents the installed capacity of device s and UC_s^{cap} denotes the unit installation cost of device s. The symbol s denotes the energy device; p denotes the service life; r denotes the interest rate which is assigned as 5%.

As defined in Eqn. (3), the *OPEX* denotes the total operation cost including the fuel cost (*FC*), maintenance cost (*MC*) as well as the grid cost (*GC*).

$$OPEX = \sum_{h} FC_h + MC_h + GC_h \tag{3a}$$

$$FC_h = \frac{E_h^{\mathrm{CHP}}}{\eta^{\mathrm{CHP}}} \times UC^{\mathrm{NG}} + \frac{Q_h^{\mathrm{Boiler}}}{\eta^{\mathrm{Boiler}}} \times UC^{\mathrm{NG}} \tag{3b}$$

$$MC_h = \left(E_h^{\mathrm{CHP}} + Q_h^{\mathrm{Boiler}} + Q_h^{\mathrm{HP}} + Q_h^{\mathrm{EC}} + Q_h^{\mathrm{AC}} \right) \times C_t^{\mathrm{maint}} + \sum_{i} P_{i,h}^{\mathrm{EV}} \times C_{\mathrm{EV}}^{\mathrm{maint}} \tag{3c}$$

$$GC_h = C_h^{\mathrm{im}} \times E_h^{\mathrm{im}} \times \phi_h^{\mathrm{im}} - C_h^{\mathrm{ex}} \times E_h^{\mathrm{ex}} \times \phi_h^{\mathrm{ex}} \tag{3d}$$

where the *FC* cost refers to the natural gas consumption of the CHP and Boiler. E^{CHP} is the power output of CHP and Q^{Boiler} denotes heat generated by the boiler, η denotes the efficiency. UC^{NG} is the unit cost of the natural gas. Symbol h denotes the current timeslot.

The *MC* comprises the annualised MC of energy technologies, which is determined by both the energy flow and the unit maintenance cost C_t^{maint}. E^{CHP} represents the electricity generated by the CHP. Q^{Boiler} and Q^{HP} denote the total heating energy generated by the boiler and heat pump (HP). Q^{EC} and Q^{AC} denotes the cooling energy generated by the electric chiller (EC) and absorption chiller (AC). $P_{i,h}^{\mathrm{EV}}$ is the charging or discharging power of EV i. Symbol i denotes the current charging EV in the timeslot h.

As given in (3c), the *GC* is determined by the cost for purchasing electricity from the grid and revenues from selling electricity back to the grid. The C^{im} and C^{ex} are respectively the tariffs for purchasing and selling electricity. The E^{im} and E^{ex} are respectively the amount of purchasing and selling electricity. The ϕ^{im} and ϕ^{ex} are the bool variables. When the purchasing electricity occurs at timeslot h, $\phi^{\mathrm{im}}=1$; otherwise $\phi^{\mathrm{im}}=0$. The same principle applies to ϕ^{ex}.

The annualised carbon emission (*ACE*) objective is formulated from the environmental perspective. The equivalent carbon emission is defined in Eqn. (4), which not only considers the direct carbon emissions from the gas combustion in the onsite devices of the CHP and boiler, but also includes the equivalent CO_2 emission from the grid purchased electricity.

$$ACE = \vartheta^{\mathrm{grid}} \times \sum_{h} E_h^{\mathrm{im}} \times B_h^{\mathrm{im}} + \vartheta^{\mathrm{NG}} \times \sum_{h} \left(\frac{E_h^{\mathrm{CHP}}}{\eta^{\mathrm{CHP}}} + \frac{Q_h^{\mathrm{Boiler}}}{\eta^{\mathrm{Boiler}}} \right) \tag{4}$$

where ϑ^{grid} and ϑ^{NG} denote the carbon emission factors regarding the grid electricity and the natural gas, respectively, which can be obtained from [41].

The model constraints refer to IES operation and V2G scheduling. The V2G-IES model should be subject to the following constraints.

Energy balances.

In the V2G-IES model, the energy balance means that the electrical, heating and cooling demands need to be satisfied. In detail, Eqn. (5) depicts the electrical balance.

$$E_{demand,h} = E_h^{\mathrm{CHP}} + E_h^{\mathrm{im}} + E_h^{\mathrm{PV}} - \sum E_{i,h}^{\mathrm{EV}} - E_h^{\mathrm{HP}} - E_h^{\mathrm{EC}} - E_h^{\mathrm{ex}} \tag{5}$$

where $E_{demand,h}$ is the electrical demand at timeslot h. E^{CHP}, E^{PV}, E^{EC}, E^{HP} denote the CHP operating power, solar power, EC operating power and heat pump power, respectively. E_i^{EV} represents the charging/discharging power of EV i. Noting that the positive E_i^{EV} represents the charging power while the negative E_i^{EV} represents the discharging power. E^{im} and E^{ex} denote the purchased and exported electricity from/to the power grid.

Eqn. (6) formulates the heating balance which mainly involves the CHP, boiler and heat hump, and the absorption chiller.

$$Q_{demand,h}^{H} = Q_h^{\mathrm{CHP}} + Q_h^{\mathrm{Boiler}} + Q_h^{\mathrm{HP}} - Q_h^{\mathrm{ACH}} \tag{6}$$

where Q^{CHP}, Q^{Boiler}, and Q^{HP} denotes the heat generated by the CHP, boiler, and air-source heat pump, respectively. Q^{ACH} represents the heat absorbed by the absorption chiller.

Eqn. (7) expresses the cooling demand which is supplied by the electric chiller and absorption chiller.

$$Q_{demand,h}^{C} = Q_h^{\mathrm{ECC}} + Q_h^{\mathrm{ACC}} \tag{7}$$

where Q^{ECC} and Q^{ACC} denote the cool energy generated by the EC and AC, respectively.

Energy conversion constraints.

The energy conversion constraints are expressed below.

$$
\begin{aligned}
E_h^{\mathrm{CHP}} &= \eta^{CHP} \cdot NG_h^{\mathrm{CHP}} \\
Q_h^{\mathrm{CHP}} &= \eta_{\mathrm{CHP}}^{\mathrm{E2H}} \cdot E_h^{\mathrm{CHP}} \\
Q_h^{\mathrm{Boiler}} &= \eta^{CHP} \cdot NG_h^{\mathrm{Boiler}} \\
Q_h^{\mathrm{EC}} &= \eta_{AC}^{\mathrm{E2H}} \cdot E_h^{\mathrm{EC}} \\
Q_h^{\mathrm{HP}} &= \eta_{\mathrm{HP}}^{\mathrm{E2H}} \cdot E_h^{\mathrm{HP}} \\
Q_h^{\mathrm{ACC}} &= \eta_{\mathrm{AC}}^{\mathrm{H2C}} \cdot Q_h^{\mathrm{ACH}}
\end{aligned}
\tag{8}
$$

where NG^{CHP} and NG^{Boiler} are the natural gas consumption of the CHP and boiler, respectively. E^{CHP}, E^{EC}, and E^{HP} are the electricity generated by the CHP, and consumed by the electric chiller and heat hump. Q^{CHP} and Q^{Boiler} are the heating supplies from the CHP and boiler. Q^{ACH} is the heat consumption from the absorption chiller. Q^{EC} and Q^{ACC} are the cooling consumption from the electric chiller and absorption chiller, respectively. η^{CHP} denotes the electricity conversion efficiency of the CHP. η^{Boiler} denotes the heating efficiency of the boiler. Besides, the η_p^k represents the conversion efficiency where the superscript "E2H" denotes the conversion process from electricity to heat and "H2C" denotes the heating to cooling conversion process.

CHP Operational constraints. The CHP is responsible for most electricity and heating demands. The start-off and operational constraints should be satisfied. The on-off constraints restrict the CHP to start only once per day which avoids the high start-up costs of the equipment- see Eqn. (9). The operational constraints contain minimum operational power (MOP) constraints (see Eqn. (10)) and ramping power (RP) constraints (see Eqn. (11)). MOP constraints avoid the CHP working under the low demand conditions and possible power drops; RP constraints avoid the drastic power variation of CHP between adjacent timeslots.

$$
\begin{aligned}
&\sum_h \chi_h^{\mathrm{CHP}} \le 1 \\
&\phi_h^{\mathrm{CHP}} - \phi_{h-1}^{\mathrm{CHP}} \le \chi_h^{\mathrm{CHP}} \le 1 - \phi_{h-1}^{\mathrm{CHP}} \\
&\chi_h^{\mathrm{CHP}} \le \phi_h^{\mathrm{CHP}}
\end{aligned}
\tag{9}
$$

where ϕ^{CHP} is a binary variable to control the on/off status of CHP and $\phi^{\mathrm{CHP}} = 1$ denotes the CHP is started. χ^{CHP} denotes a binary variable which ensures that only once switching is allowed in a day.

$$E_h^{\mathrm{CHP}} \le \phi_h^{\mathrm{CHP}} \times M_{upper}^{CHP}$$
$$E_h^{\mathrm{CHP}} \ge \left(1-\phi_h^{\mathrm{CHP}}\right) \times M_{upper} + MOP \times CAP^{\mathrm{CHP}} \tag{10}$$

where CAP^{CHP} is the installed capacity of CHP and M_{upper} denotes the upper boundary of CHP capacity. MOP is the minimum operational power factor.

$$E_h^{\mathrm{CHP}} - E_{h-1}^{CHP} \le RP \times CAP^{CHP}$$
$$E_{h-1}^{\mathrm{CHP}} - E_h^{\mathrm{CHP}} \le RP \times CAP^{\mathrm{CHP}} \tag{11}$$

where RP denotes the ramping power constraints factor.

Grid operational constraints. The electricity purchasing from and fed back to the power grid should satisfy the following grid operational constraints as illustrated in Eqn. (12).

$$0 \le E_h^{\mathrm{im}} \le \phi_h^{\mathrm{im}} \times M_{upper}^{\mathrm{grid}}$$
$$0 \le E_h^{\mathrm{ex}} \le \phi_h^{\mathrm{ex}} \times M_{upper}^{\mathrm{grid}} \tag{12}$$
$$\phi_h^{\mathrm{im}} + \phi_h^{\mathrm{ex}} \le 1$$

where E^{im} and E^{ex} are electricity been imported from the grid and exported to the grid. ϕ^{im} and ϕ^{ex} are the binary variables which denote the interaction status (purchasing and exporting) with the power grid. $M_{upper}^{\mathrm{grid}}$ is the maximum power exchange with the grid.

EV charging constraints

For the practical application in the real world, EV charging should satisfy some constraints including the charging power constraints (Eqn. (13a)), battery SOC constraints (Eqn. (13b)) as well as the final electricity requirement (Eqn. (13c)) for traveling.

$$-E^{\max} \le E_h^{\mathrm{EV}} \le E^{\max} \tag{13a}$$

$$0.1 \le SOC_{ini} + \sum_{h \in \mathbb{R}} E_h^{\mathrm{EV}} / CAP^{\mathrm{EV}} \le 1, \ \forall h = 1, 2 \cdots R \in \mathbb{R} \tag{13b}$$

$$SOC_{ini} + \sum_{h \in \mathbb{R}} E_h^{\mathrm{EV}} / CAP^{\mathrm{EV}} \ge 0.9 \times CAP^{\mathrm{EV}} \tag{13c}$$

where E_h^{EV} denotes the charging/discharging power at timeslot h; SOC_{ini} represents the SOC of batteries; CAP^{EV} is the battery capacity and $\mathbb{R}$ denotes the available set of charging timeslots. Eqn. (13a) constrains the charging and discharging power. Constraints in Eqn. (13b) prevent EVs from being over-charged or over-discharged at any timeslot h. Eqn. (13c) ensures that EVs can be charged to at least 90% of battery capacity before the departure, which

ensures the traveling demands. Note that every individual EV should satisfy the above constraints.

2.3 EV charging settings

This study simulates 120 EV participating in V2G-IES. The battery capacity of each EV is assumed as 25 kW, and the charging and discharging power are bounded within 8 kW. The EV always charges or discharges the battery in a constant power for a scheduling hour from its arrival to the charging pipe until its departure. The overall charging process should satisfy the basic principle of EVs, i.e. before the departure of EVs, batteries should be charged as least 90% of state of charge (SOC) to ensure the basic travel demands and at any time, the battery should have at least 10% of electricity for the battery health consideration [42]. If the battery electricity is less than this threshold, the self-protection program of battery management system should be activated and stop the discharging operation.

The battery SOC is defined in Eqn. (14) which is determined by the charging power and charging duration.

$$SOC_{cur} = SOC_{ini} + \sum_{h} E_h^{\mathrm{EV}} \times T_s \Big/ CAP^{\mathrm{EV}} \tag{14}$$

where SOC_{ini} and SOC_{cur} are the initial and current SOC values of batteries. E_h^{EV} denotes the charging or discharging power at timeslot h and CAP^{EV} represents the battery capacity. T_s is the length of a time slot and it is one hour in this study.

The stochastic features of V2G schedule are reflected in three aspects, i.e., the charging start time, charging duration, and the initial battery state. The EV traveling characteristics in commercial and residential cases are different. The distribution probability of charging start

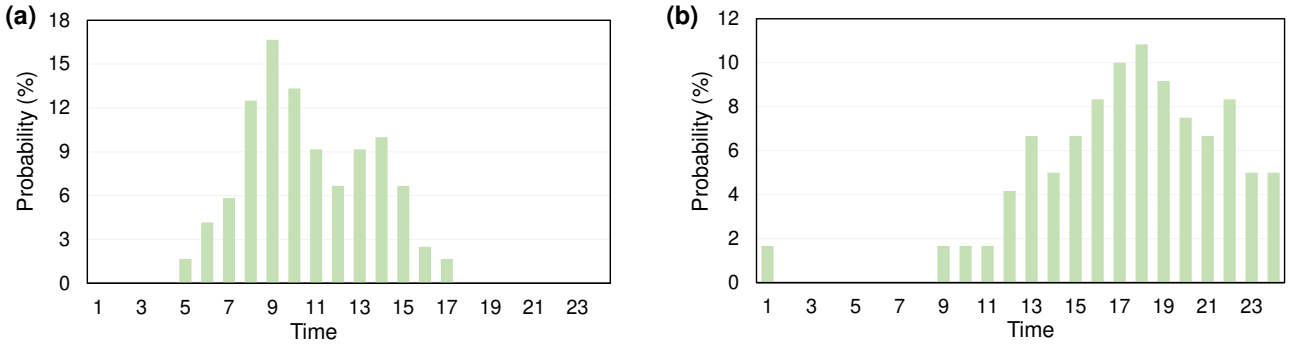

Fig. 3 The distribution probability of charging start time for EVs in the commercial case (a) and residential case (b).

time for EVs in the commercial and residential areas are illustrated in **Fig. 7** (a) and (b), respectively, based on the National Household Travel Survey (NHTS) [43]. In commercial cases, the charging mainly starts in the morning (i.e., arrival time of EVs) and lasts during the daylight. While in residential cases, the charging process mainly distributes in the night and the charging duration is larger than that in commercial cases. Explicitly, the EV arrival time (i.e., charging start time) in commercial cases is concentrated between 7 a.m. ~ 3 p.m. while the EV arrival time in residential case is mainly distributed between 12 p.m. ~ 12 a.m.

Accordingly, the duration of EV charging in the commercial and residential cases are 5~10 h and 7~13h as depicted in Eqn. (15).

$$X_{comm} \sim N(7.5,1), \quad X_{comm} = clip(5,10) \tag{15a}$$

$$X_{res} \sim N(10,1), \quad X_{res} = clip(7,13) \tag{15b}$$

where X_{comm} and X_{res} are the probability distribution function of the charging duration for EVs in the commercial and residential cases, respectively. $X \sim N(\mu, \sigma^2)$ represents that the probability of charging duration follows the Gaussian distribution function with the expectation μ and variance σ^2. Symbol "$\mathrm{clip}(lb, ub)$" denotes the clip operation which restricts the charging duration time situated in a reasonable range between lower boundary "*lb*" and upper boundary "*ub*" [44]. Meanwhile, the initial SOC of the batteries is uniformly distributed between 0.15~0.3, as shown in Eqn. (16).

$$SOC_{ini} = random(0.15,0.3) \tag{16}$$

2.4 Model solving

To capture the V2G-IES performance trade-off between the cost and emissions objectives, as well as considering the complicated constraints on the EV charging, the non-dominated sorting genetic algorithm II (NSGA-II) [45] is adopted to solve the V2G-IES model and assess the trade-off by plotting the Pareto frontiers. During the model solving, two computational challenges emerge for the typical NSGA-II algorithm as follows.

(1) Since the V2G-IES optimisation model has multi-dimensional and mix-integer constraints, the model solving with traditional NSGA-II could easily been trapped into the local optima.

(2) The whole computational process could be time-consuming if the first generation of particles are randomly initialised.

To address the model-solving challenges, we introduce the diversity maximization (DM) heuristics (i.e. Eqn. (17~18)) to initialise the particle population and form the feasible set E which demonstrates better performance than the traditional NSGA-II algorithm in addressing the local optima and computational-time challenges [46]. The schematic illustration of the DM-NSGA-II algorithm is depicted in **Fig. 3**. The diversity measure α_E of objectives are defines below.

$$\alpha_E(y) = \max_{y_e \in E} \left(\min \frac{y^{(i)} - y_e^{(i)}}{\Delta_{ie}} \right) \tag{17a}$$

$$\Delta_{ie} = \max_{y_e \in E} \ y_e^{(i)} - \min_{y_e \in E} \ y_e^{(i)} \tag{17b}$$

where the diversity measure α_E indicates the diversity degree between different solutions and Δ_{ie} denotes the maximum difference among the particle populations, which is utilised to normalise the objectives. Symbol i in this equation denotes the objective number. The feasible solutions can be obtained successively through the synchronous iteration of α_E, see Eqn. (18).

$$\min Z = \min_X \left(\alpha_E(y), \sum_{j=1}^{K} \omega_j y^{(i)} \right) \tag{18}$$

where X is the decision variables and ω_j is the positive weight factor. Taking the feasible solution E as the initial particle swarm of the NSGA-II algorithm can enable the optimisation process to approach near the Pareto frontier, thereby reducing the iteration time and avoiding the possible local optima traps. Then, the logic flow of the NSGA-II algorithm is described.

(1) **Calculating the crowding distance and the nondominated sorting.** The crowing distance of particles is calculated. Then, the rank of individual particles is determined and the particles are sorted according to their priorities.

(2) **Game selection.** The tournament game strategy will choose two populations to take part in the subsequent crossover and mutation processes. The principle of game selection is that particles with high priority and large crowding distance will be firstly adopted.

(3) **Crossover and mutation.** The simulated binary crossover and polynomial mutation strategy are utilised to generate the new offspring population maintaining the diversity of particles and accelerating the optimum searching process.

(4**) Population recombination.** The parent and offspring populations are combined and thereby a new generation is generated for the next elite selection.

(5) **Nondominated sorting.** The distance between particles in the new generation is calculated and the sorting process is executed according to the priority of particles like the step (1).

(6) **Elite selection and generation of new population.** The elite selection strategy is adopted to choose a new generation from the recombined populations, where the particles with the high rank and large crowding distance are selected.

The iteration from (1) to (6) enables the particles to approach the Pareto frontier and each particle represents a set of decision variables denoting the system installed capacity, the operation status, and the charging power of EVs. More details of DM-NSGA-II algorithm are available in our previous research [47].

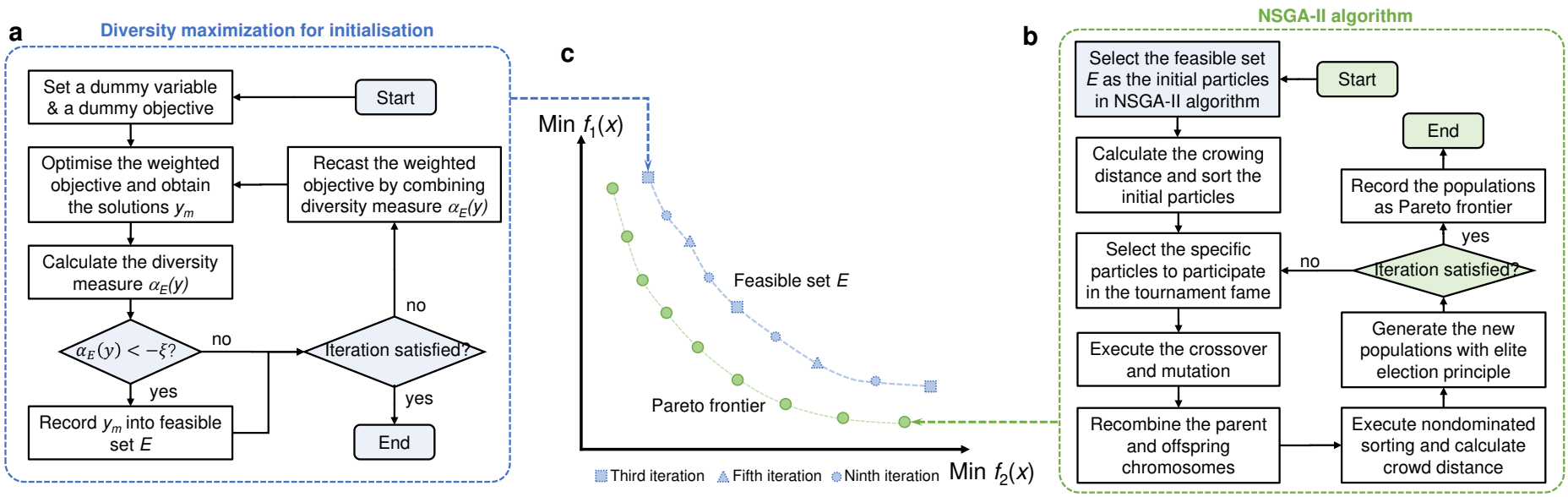

Fig. 4 The proposed DM-NSGA-II algorithm for solving the V2G-IES optimisation model. a) Diversity maximization heuristics to form the initialised feasible set E which is closer to the Pareto frontier; b) DM-NSGA-II algorithm solves the multi-objective optimisation problem; c) Illustration of the initialised feasible set E and the final Pareto frontier.

2.5 Decision making

The Pareto frontier provides a set of non-dominated solutions regarding to the economic and environmental performances. For a practical application, only one optimal solution could be selected and built, which leads to a multiple-criteria decision making problem. In this study, the "Euclidean-distance" based TOPSIS method [48] is adopted to identify the overall best solution from the Pareto frontier as described below. This method is utilized to find the best optimal solution in the Pareto frontier. In other word it is to find the most balanced point where both objectives can be sufficiently evaluated.

The normalisation of two objectives is executed firstly to place all the objectives into a same dimension scale between 0-1 as shown in Eqn. (19).

$$f_{ij}^{norm} = \frac{f_{ij} - \min\left(f_{ij}\right)}{\max\left(f_{ij}\right) - \min\left(f_{ij}\right)} \tag{19}$$

where the subscript (*ij*) denotes the *j-th* solution in the *i-th* objective. With the normalised objectives, the TOPSIS decision making method can be utilised. The details are illustrated in **Fig. 4**, where the "ideal" and "nadir" points indicate the absolute optimum point and the worst point theoretically. The Euclidean distances from the non-dominated solutions to the "ideal" and "nadir" points can be determined accordingly as marked by ED_{i+} and ED_{i-},

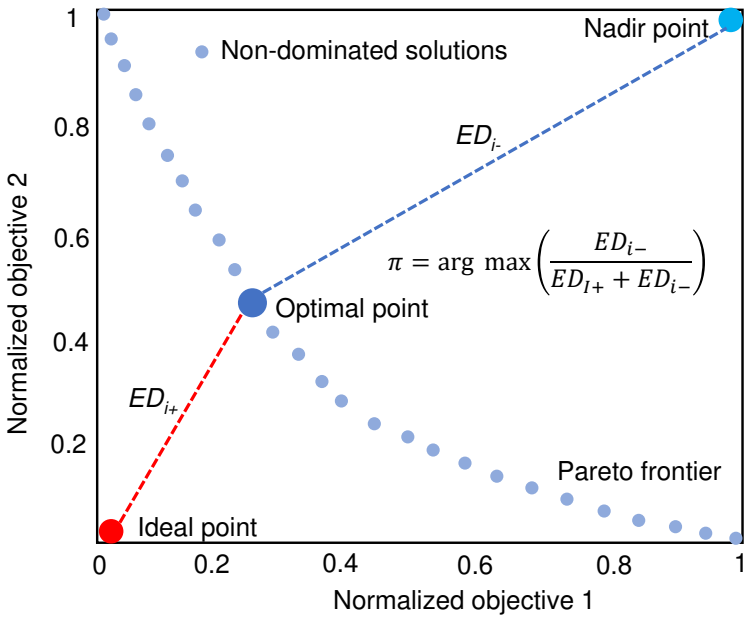

Fig. 5 Illustration of Pareto-optimality and posterior decision making to identify one overall solution on the Pareto frontier.

respectively, in Eqn (20).

$$ED_{i+/i-} = \sqrt{\sum_{j=1}^{n}\left(f_{ij} - f_j^{ideal/nadir}\right)} \tag{20}$$

The smaller ED_{i+} indicates that this solution is closer to the ideal optimality, and vice versa. Similar principle can be applied to the ED_{i-} pursuing the maximum value. Then, the index π is defined to find the overall best solution from the Pareto frontier as expressed in Eqn. (21).

$$\pi = \arg\ \max\left(\frac{ED_{i-}}{ED_{i+} + ED_{i-}}\right) \tag{21}$$

3 Case study setups

3.1 Overview

In this study, the proposed V2G-IES optimal planning framework is applied to six cases as defined in **Fig. 5**. Three cities of Beijing, Shanghai and Xiamen in China are selected representing three typical climate conditions with different cooling/heating demands, i.e., "Moderate summer, cold winter" in Beijing, "Hot summer, cold winter" in Shanghai and "Hot summer, moderate winter" in Xiamen. Meanwhile, energy prices and the carbon emission factors could be different for each city. Then, two types of functional areas, i.e., commercial and residential areas, are considered in each city as different functional areas have significantly different energy demand profiles. Three scenarios, i.e. IES only, IES+G2V, and IES+V2G, are further compared for each case to demonstrate the benefit of embedding V2G into IES. The scenario "IES only" denotes the original IES without the V2G applications. "IES+G2V" scenario means that EV only charge the battery from the grid with an average power which is the current charging mode in the real world. Note that the case studies in three cities of China have been performed to validate our modelling and methods, while our proposed model and method are generally applicable for other countries and cities.

In each city, three typical seasons of summer, winter, and transition seasons (i.e. spring and fall) are modelled. Cooling is needed in summer and heating is needed in winter, while transition seasons have less cooling and heating demands. **Fig. 6** presents the electrical, cooling and heating demand profiles for the six cases. The electrical demands for all seasons

are similar in one case. Beijing has a larger heating demand and less cooling demand; Xiamen has a little heating demand but a larger cooling demand; Shanghai has the moderate heating and cooling demands compared with the other cities.

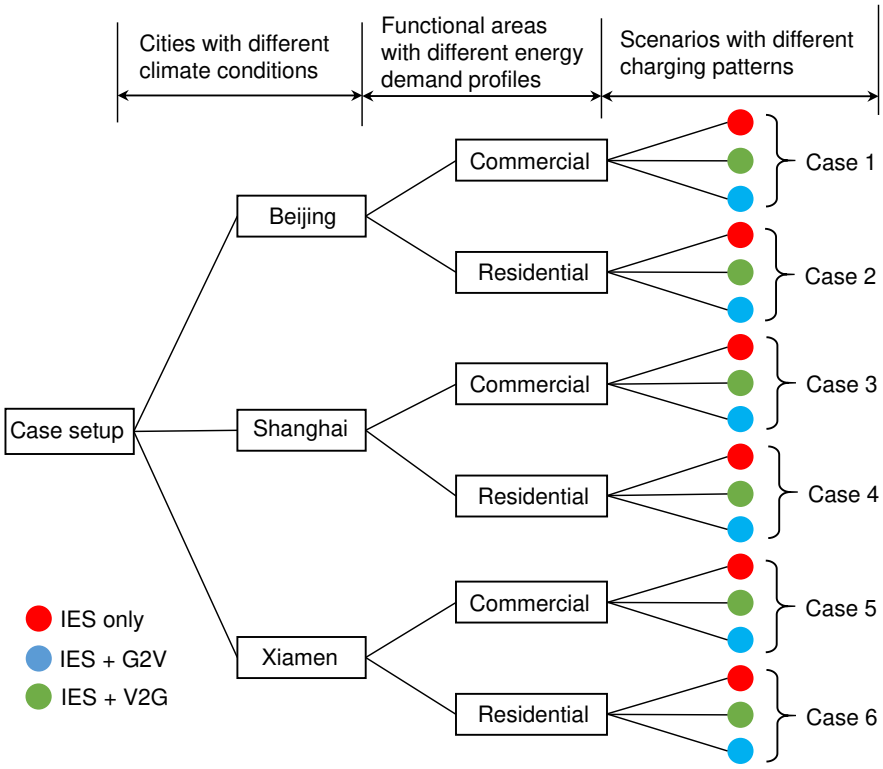

Fig. 6 Scenario and case settings in this study with three locations , two functional areas and three different charging patterns.

3.2 Inputs database and pre-processing

The technical inputs regarding to each technology's efficiency and operation are presented in **Table A2**. The upper bounds of the installed capacity of each technology are also listed in this table, which is applied in the optimisation model to constrain the system planning and operation. Economic inputs including the unit capital cost and maintenance cost of each technology are presented in **Table A2**. The energy price and the feed-in tariff of each case are illustrated in **Fig. A1**. The emission factors for the grid electricity and gas consumption are listed in **Table A2**. The rest parameters are detailed in **Appendix A1**.

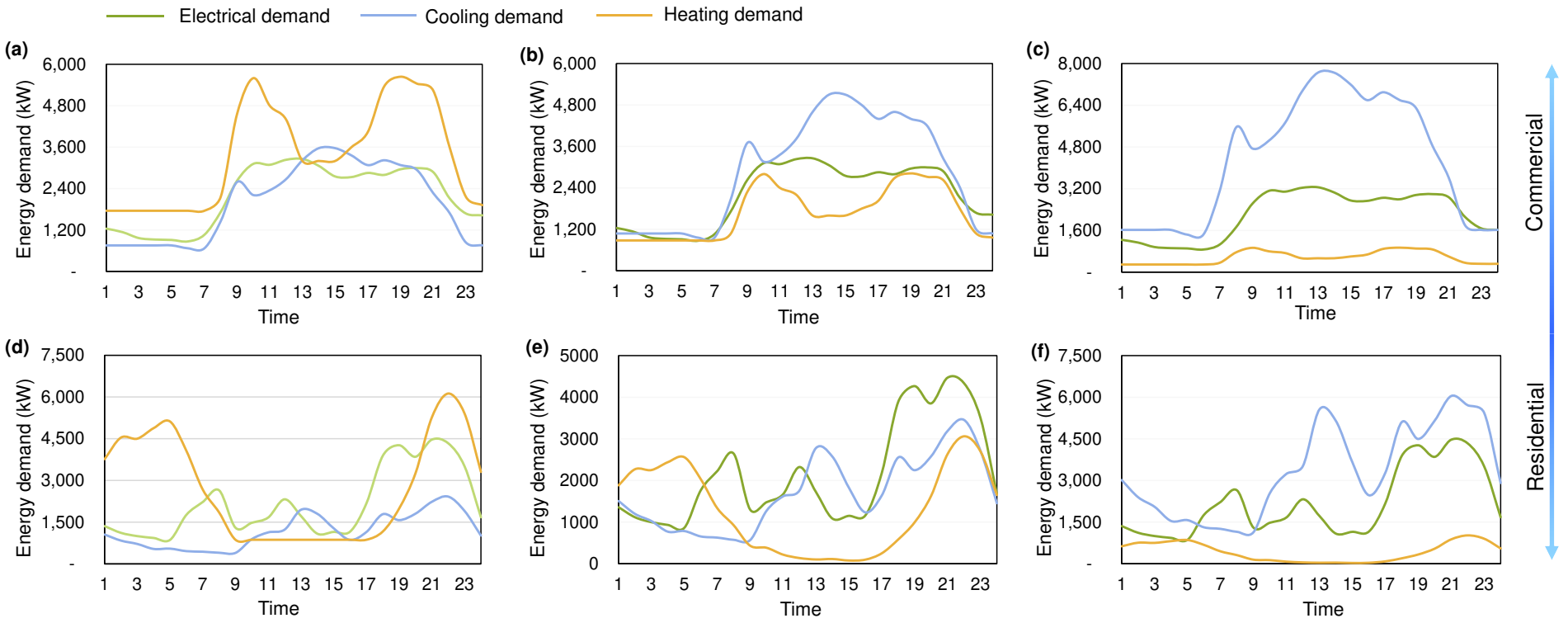

Fig. 7 Electricity, cooling, and heating energy demand profiles for six cases. (a) Beijing commercial; (b) Shanghai commercial; (c) Xiamen commercial; (d) Beijing residential; (e) Shanghai residential; (f) Xiamen residential.

3.3 Modelling environment

The proposed V2G-IES model and the model solving method of DM-NSGA-II algorithm are coded in MATLAB 2020b on a PC with the Intel (R) Core (TM) i7-8565 CPU @ 1.8 GHz and 8.0 GB of RAM.

4 Results and discussions

4.1 Whole system performance when introducing V2G into IES

The trade-off between system costs and carbon emissions in six cases when introducing V2G into IES is illustrated by Pareto frontiers in **Fig. 8**. For all cases no matter integrating V2G into IES or not, due to the high investment of EV charging infrastructure, the “IES only” scenario achieves less ATC and ACE than both the “IES+V2G” and “IES+V2G” scenarios. While the “IES+V2G” scenario exhibits better cost and emission performance than those of “IES G2V” scenario, which indicates V2G, as a flexible storage, could contribute the IES performance. The Pareto frontiers of “IES+V2G” locates somewhere between those of “IES only” and “IES+G2V”. The “IES+V2G” Pareto frontier is relatively closer to the “IES only” Pareto frontier than the “IES+G2V” Pareto frontier, indicating that V2G could bring more benefits to the IES. Specially, the “IES+V2G” applications in Beijing commercial, Shanghai commercial, Shanghai residential could achieve more significant cost and emission reductions compared to the “IES+G2V”. For the rest cases, introducing V2G would not bring significant benefits.

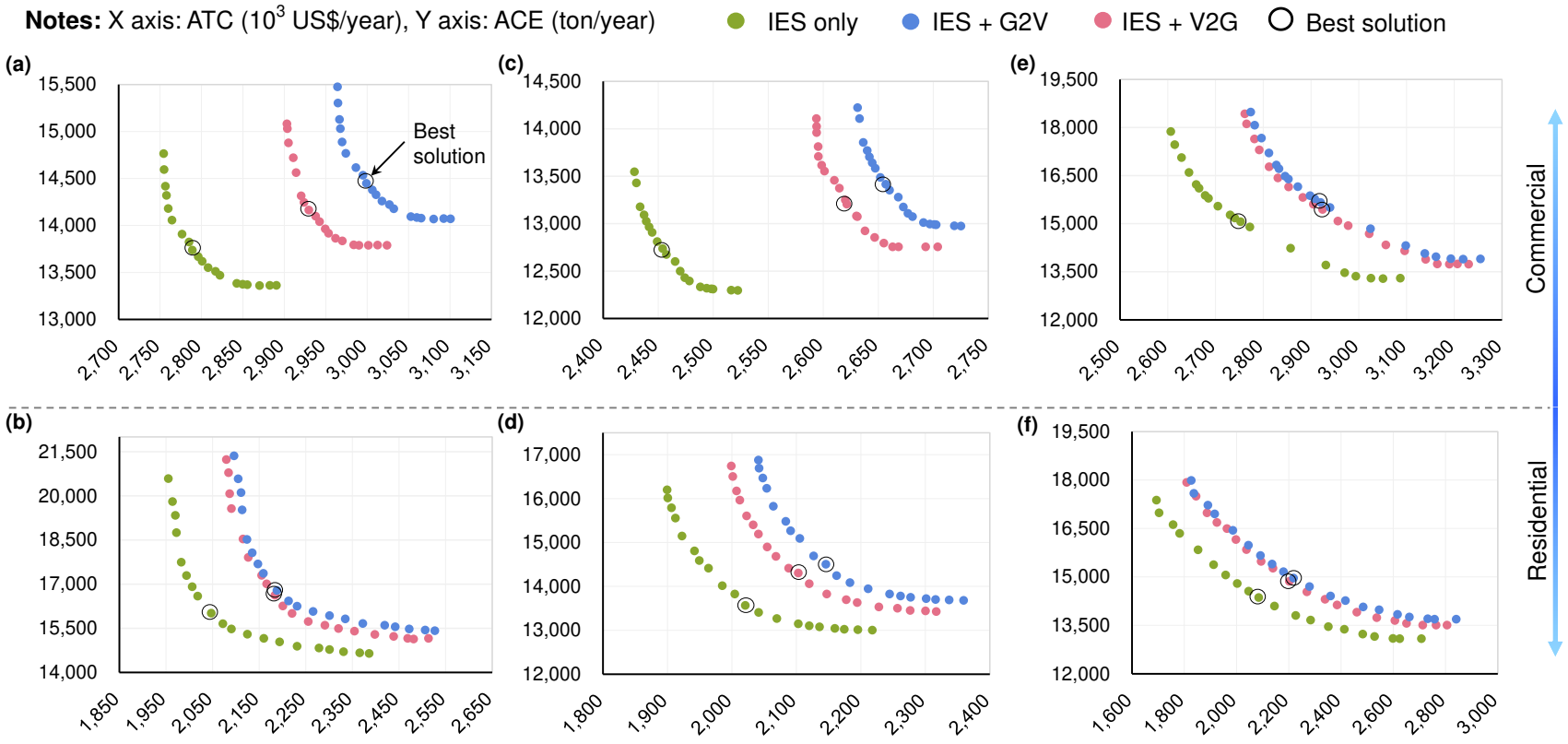

Fig. 8 Pareto frontiers representing the design trade-off between the least cost and emissions objectives in six cases. (a) Beijing commercial, (b) Beijing residential, (c) Shanghai commercial, (d) Shanghai residential, (e) Xiamen commercial, (f) Xiamen residential.

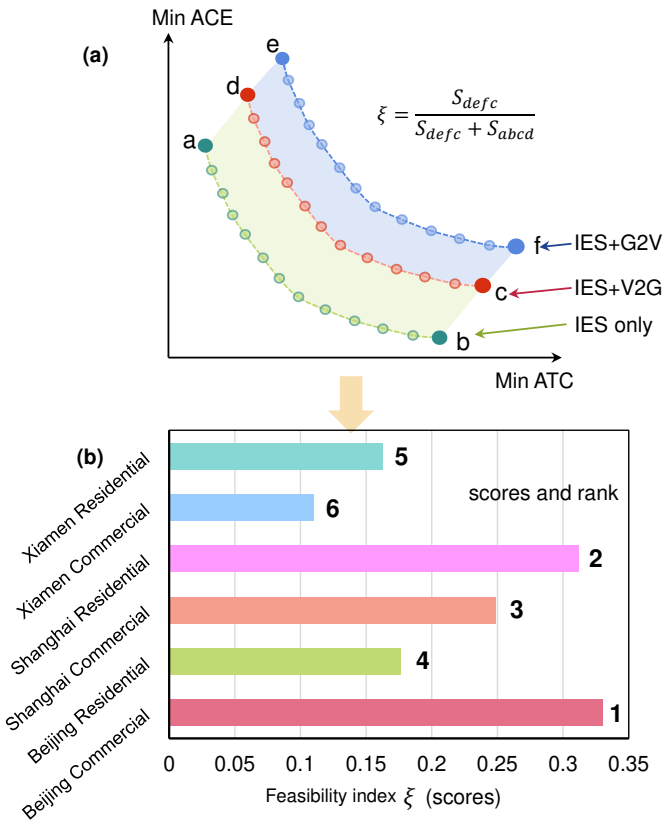

Fig. 9 Quantifying the performance improvement induced by V2G in six cases. (a) Evaluation criterion, (b) Scores and ranks for six cases.

To further quantify the benefit of introducing "IES+V2G" in different cases, we propose the area-based evaluation indicator, namely, feasibility index ξ. The schematic diagram and corresponding results are illustrated in **Fig. 9**. The mathematical expression of feasibility index is defined as:

$$\xi = \frac{S_{defc}}{S_{defc} + S_{abcd}} \tag{22}$$

where S_{defc} denotes the normalized area enclosed by the "IES+V2G" Pareto frontier curve and the "IES+G2V" Pareto frontier curve while S_{abcd} denotes the normalized area enclosed by the "IES+V2G" Pareto frontier curve and the "IES only" Pareto frontier curve.

The feasibility index indicates that the "Beijing commercial" case achieves the best performance, followed by the "Shanghai residential" case. In contrast, the V2G application in Xiamen city has no remarkable improvement than the G2V scenario. This indicates Beijing and Shanghai are more desired locations to demonstrate the integration of V2G into the IES. Hence, we further choose the "Beijing commercial" case to analyse the impact of V2G as a

flexible storage on IES design and dispatch in the following sections. It is noted that the feasibility is comprehensively affected by the energy demand patterns, the energy demand ratio, and the energy prices.

4.2 Impacts of V2G on IES design and operation

4.2.1 IES installed capacity

The impact on IES design induced by V2G in "Beijing commercial" case is visualized in **Fig. 10**, in which the "IES only" system design is in red and the IES design with V2G is in green. The technologies' installed capacities vary from the CO_2 emission optimum to cost optimum. Several observations are as follows.

(1) Seen from **Fig. 10** (a), in the "IES only" scenario, the installed capacity of combined heating and power (CHP) gradually decreases from 3,500 kW to 3,000 kW with the objective moving from emission optimum to cost optimum. This phenomenon can be partially explained by the natural-gas-based CHP offers cost-competitive design options but may produce more CO_2 emissions. By contrast, V2G increases the total technologies' capacity of CHP by about 100 kW, which occurs due to the increased electric demand from EV fleets.

(2) As shown in **Fig. 10** (b), to realise the cost optimality, the installed capacity of boiler gradually increases and stabilises at around 1,900kW. The adoption of V2G does not significantly increase the installed capacity of boiler. When pursuing the economic optimality, the boiler's capacity is relatively stable around 1,900 kW regardless of whether V2G is introduced. Along with the increase of boiler capacity, more heats are generated by the boiler, a decrease of heat hump's installed capacity can be observed accordingly in **Fig. 10** (c).

(3) The installed capacity of absorption chiller (AC) is shown in **Fig. 10** (d). It can be seen that with the V2G, the total installed capacity of AC is enlarged by roughly 300 kW. When the objective function moves from emission optimality to cost optimality, the installed capacity tends to decrease, whose tendency is more obvious in the "IES+V2G" scenario. As the AC installed capacity gradually decreases, an increase in electric chiller (EC) capacity is observed to satisfy the cooling demand. However, it is noteworthy that the design for the emission optimality is apt to not install EC. This can be explained by the "IES+V2G" scenario tends to install even larger capacity of CHP with more amount of extra heats that can be utilised to produce sufficient cooling during summer.

(4) The photovoltaic (PV) panel installed capacity remains the same no matter the cost and emission objective functions, and no difference can be found in “IES only” and “IES+V2G” scenarios. This is mainly because PV panels are a type of clean and economic-efficient technology.

4.2.2 IES dispatching

The impact of V2G on the IES dispatch is illustrated by utilising hourly electricity, heating and cooling balances in the “Beijing commercial” case as shown in **Fig. 11** and **Fig. 12**, respectively.

For electricity balance in “IES+V2G” scenario, the CHP and the grid synergistically satisfy the electrical demand in summer. In the transition seasons, only the grid is responsible for the electricity demand as shown in **Fig. 11** (c) and (d), during which the heating and cooling demands are at low values, thereby operating the CHP is not economic. In contrast, to fulfil the relatively higher heating demand in winter, the CHP predominately provide the electrical demand and surplus electricity generated by CHP could be feed back to the grid (**Fig. 11** (e)). Compared with the “IES only” scenario, V2G intervention would enlarge the total electrical demand which is covered by larger output of the CHP during 3-6 p.m. and 7-10 p.m.

Meanwhile, the V2G charging powers distribute differently in different seasons. Explicitly, in summer (**Fig. 11** (a)), the EV would charge or discharge following the time-of-use tariff, i.e., the charging process concentrates in the off-peak period of 2-5 p.m. and the discharging process happens during the peak period of 10-1 p.m. and 6-8 p.m. This tendency is more apparent in the transition season scenarios, during which the grid fulfils all electrical demand, and from the economic point of view, EV fleets are inclined to charge the batteries during the valley-period and discharge the batteries’ energy back to the grid for more revenues during the peak-period. By contrast, in winter as shown in **Fig. 11** (e), the charging power is more evenly distributed during 7 a.m. to 10 p.m. This is because only CHP system provides the electricity and thus the EV fleet will charge or discharge the batteries following the CHP’s output with few impacts from the grid electricity price.

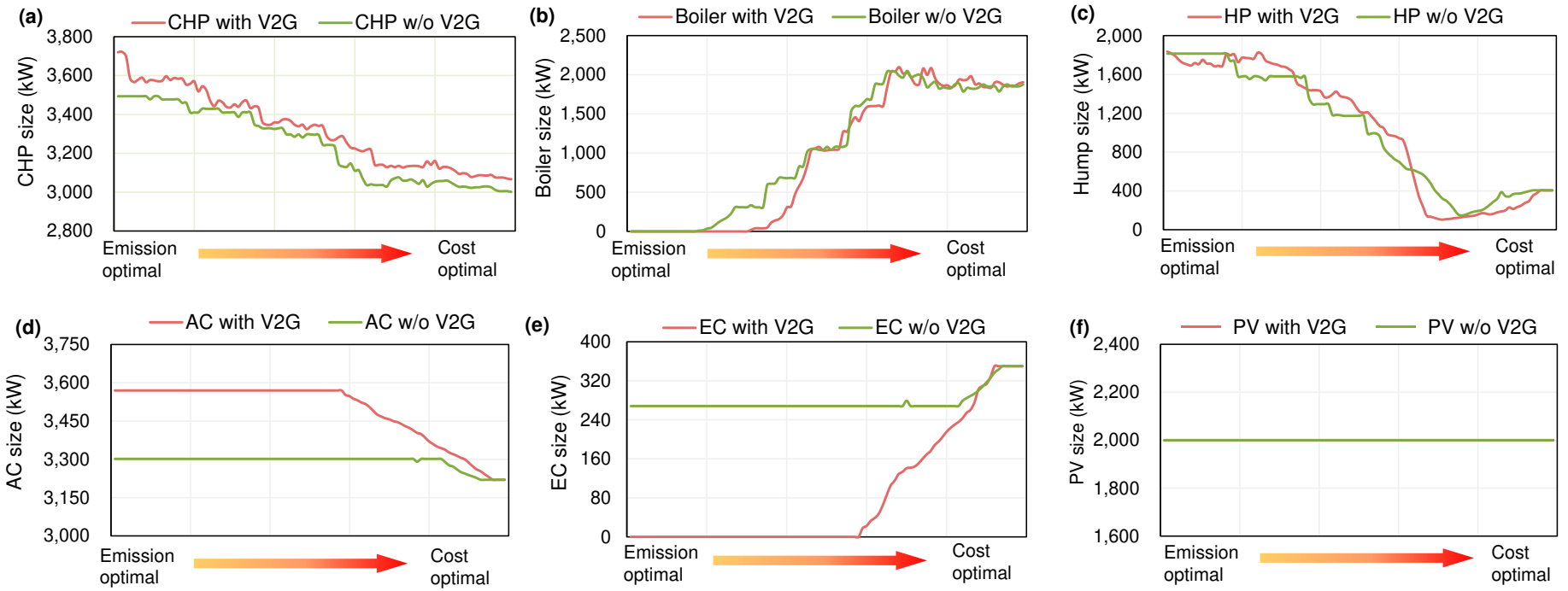

Fig. 10 Energy technologies' installed capacities varying with objective functions with/without V2G. (a) CHP, (b) Boiler, (c) Heat pump (HP), (d) Absorption chiller (AC), (e) Electric chiller (EC), (f) Photovoltaic (PV) where two curves overlap.

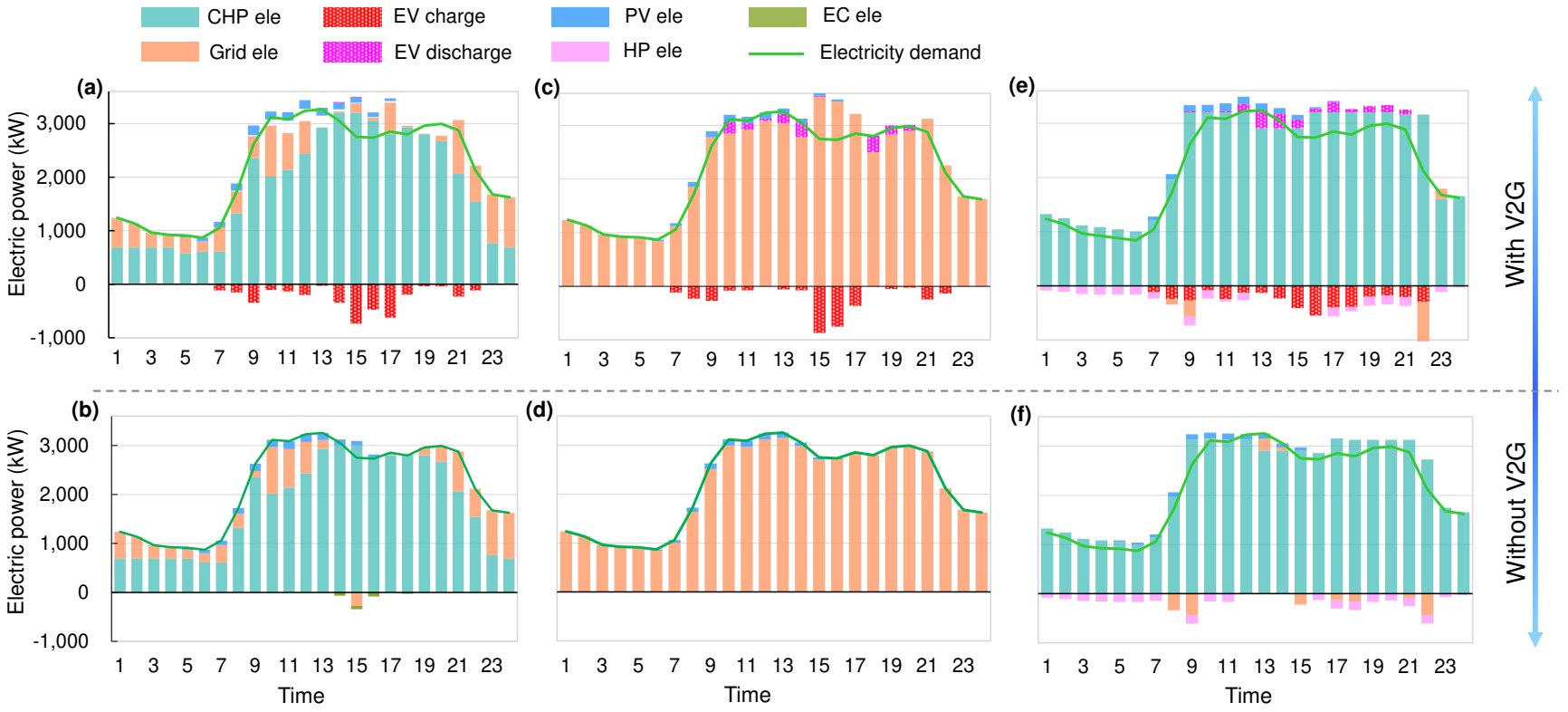

Fig. 11 Electricity balancing in different seasons for the decision-making solution. (a) Summer with V2G, (b) Summer without V2G, (c) Transition seasons with V2G, (d) Transition seasons without V2G, (e) Winter with V2G, (f) Winter without V2G.

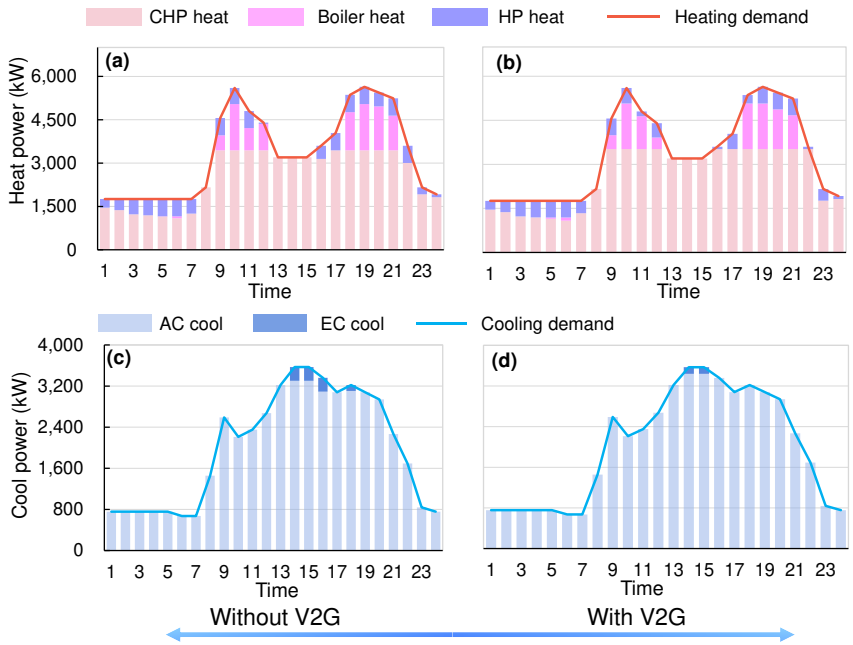

Fig. 12 Heating and cooling balance for the decision-making solution in Beijing commercial case. (a) Heating balance without V2G in winter, (b) Heating balance with V2G in winter, (c) Cooling balance without V2G in summer, (d) Cooling balance with V2G in summer.

The heating and cooling balances are illustrated in **Fig. 12**. The heating demand is mainly fulfilled by the CHP and the boiler during 9-12 p.m. and 6-9 p.m. The output of heat pump is relatively stable, which acts as an effective supplement to other heat sources. The cooling demand balances as shown in **Fig. 12** (c) and (d) show that most of cooling demand is covered by the absorption chiller, while the electric chiller contributes a little. Comparatively, the introduction of V2G application make a little difference to the heating and cooling balances. In general, the adoption of V2G reduces the output from the heat pump and EC, which can be found at 10 p.m. in **Fig. 12** (b) and 2-6 p.m. in **Fig. 12** (d). This can be partially explained by that the CHP would output more to fulfil the requirement of EV charging, and the heating output of CHP is also increased, which consequently reduces the heating output from the heat pump. Furthermore, more heating can be utilised for cooling by the absorption chiller (AC), which results in the less EC usage.

4.3 EV scheduling

This section discusses the scheduling of EVs and validates the EV charging functions in the Beijing commercial case. We choose 10 typical EVs from 120 EVs to analyse the EV charging characteristics. These EVs features different initial SOC from 0.15-0.3. Their charging or

discharging periods distribute between 7 a.m. and 10 p.m. and are encircled with magenta box **Fig. 13** (a)-(c), the corresponding SOC curves of 10 EVs are presented in **Fig. 13** (d)-(f).

During 3-5 p.m. in summer, all EVs tend to charge their batteries due to the lower electricity price, and this phenomenon is much more obvious in transition seasons since all electricity only comes from the grid. By contrast, EVs in winter (**Fig. 13** (c)) charge their batteries much evenly since most of the electricity demand in winter is satisfied by the CHP and the charging process would not be affected by the time-of-use grid tariff significantly. In general, the switch between charging or discharging is less than three times, which avoids the frequent switching between positive and negative currents and ensures the battery health. According to the SOC curves, the final SOC of batteries are all over 90%, which further satisfies the charging requirements of EVs. More interesting observations are as follows.

(1) The charging state of EVs varies greatly with the charging period distribution. Taking "EV1" and "EV4" in summer (**Fig. 13** (d)) as an example, EV1 tends to charge enough energy from 7 to 9 a.m. and then feed the surplus energy when the system requires more electricity during 9-11 a.m. By contrast, EV4 discharges the battery to IES initially at 10 am and then from 1 p.m., it starts to charge the battery until the battery is fully charged. The main reason derives from the initial SOC of vehicles. For instance, the initial SOC of EV1 is low and it has to charge enough for the subsequent V2G function. This phenomenon presents that the practical charging or discharging behaviour of EVs would adaptively regulate according to the battery state and the IES state.

(2) The charging power varies with the seasons. Taking EV1 as an example, EV1 in summer (**Fig. 13** (d)) would charging the battery according to the electric demand as mentioned before. However, the charging state in winter (**Fig. 13** (f)) is significantly different, during which the EV1 would directly charge up to full state and then keep up to the end without the discharging state. This is because the CHP is the only electricity provider in winter, EVs can be relatively flexible to charge the battery regardless of the electricity price and the electrical demand.

All these phenomena reveal that the EVs can offer the flexibility of energy storage to the IES by regulating the charging/discharging states according to the electrical demand and the time-of-use electricity tariff.

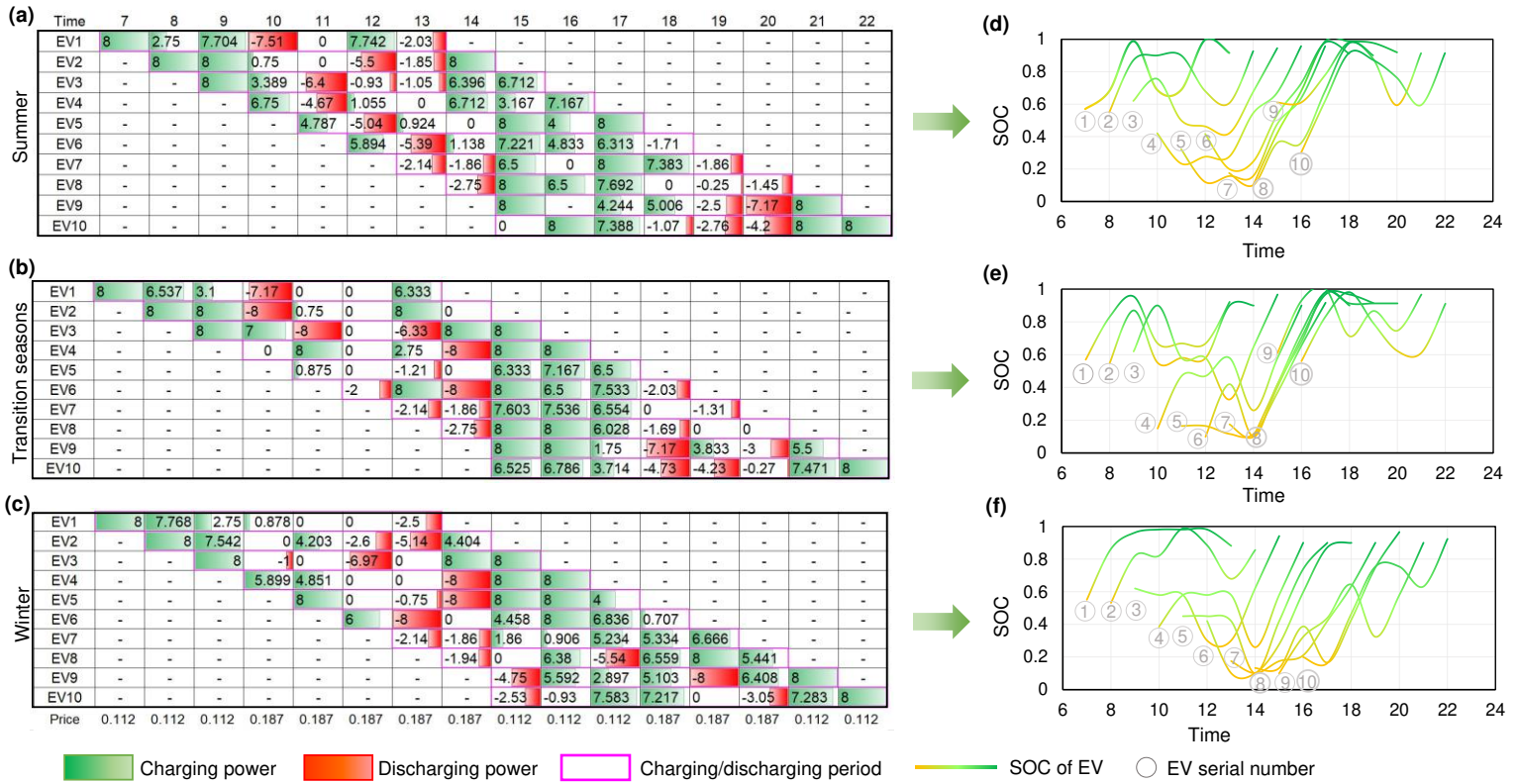

Fig. 13 EV scheduling in different seasons for the Beijing commercial case. (a)-(c) EV scheduling power in summer, transition seasons and winter, respectively, where negative values in red indicate discharge, positive values in green denote charge (d)-(f) Battery SOC curves, where No.1-10 denote 10 EVs.

4.4 Experimental sensitivity analysis

The uncertainties of the energy prices (including the time-of-use tariff, feed-in price, and gas price) and EV penetrations are investigated in this study, taking the Beijing commercial case as the example.

4.4.1 Energy price uncertainties

To investigate the impacts of the energy price uncertainties on the V2G-IES, three different price uncertainties are developed, including those in the electricity buying price (i.e. time-of-use tariff from the grid), feed-in price, as well as the natural gas price. The trade-off solutions and their variations with different price uncertainties have been presented in **Fig. 14** (a), (c) and (e). Seen from these series of Pareto frontiers, the price uncertainties predominately impact the annualized total cost (ATC) more than the annualized carbon emission (ACE). Explicitly, with the increase in the prices of electricity-buying, shown in **Fig. 14** (a) and natural gas, shown in **Fig. 14** (c), the ATC increase significantly while the feed-in price **Fig. 14** (e) does not affect the ATC objective significantly. This can be explained by that with the V2G application, more electricity is required inside the V2G-IES and less amount of surplus electricity is fed back to the grid.

Fig. 14 (b), (d) and (e) illustrates the capacity configuration with the different price uncertainties. Although two objectives vary with the energy prices, the installed capacities of the core CHP stay relatively stable at around 3200 kW. Noticeably, apart from the large variation in the heating pump in the **Fig. 14**(b), the installed capacities of other energy technologies basically fluctuate within an acceptable range, which implies that the system model possesses the good robustness on the energy prices.

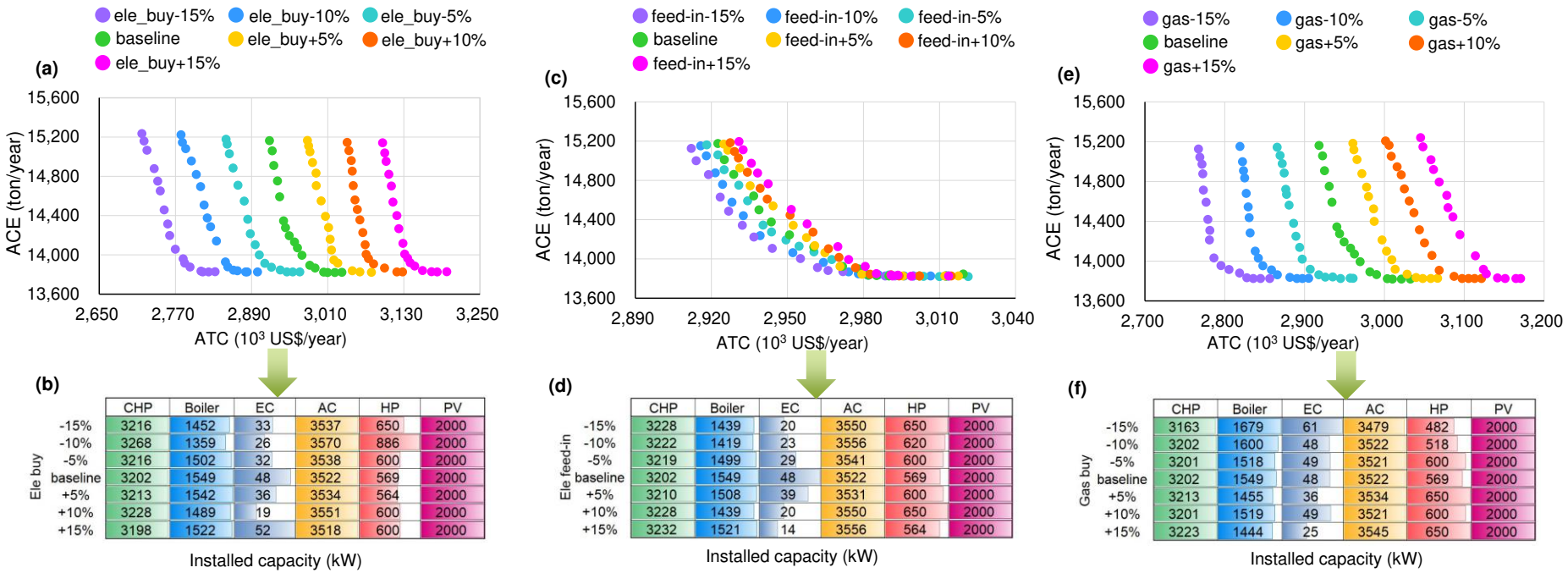

Fig. 14 Sensitivity analysis for uncertainties of electricity-buying price, feed-in price, and natural gas price in the Beijing commercial case. (a) Pareto frontiers under the electricity-buying price uncertainty, (b) Installed capacity under the electricity-buying price uncertainty, (c) Pareto frontiers under the feed-in price uncertainty, (d) Installed capacity under the feed-in price uncertainty, (e) Pareto frontiers under the gas price uncertainty, (f) Installed capacity under the gas price uncertainty.

4.4.2 EV penetration uncertainty

The EV penetration rate might potentially affect the ATC and ACE performances. The sensitivity analysis on the number of EVs from 120-480 was carried out. **Fig. 15** illustrates the system performance trade-off between ATC and ACE varying with different EV quantities. The Pareto frontier for 120 EVs is regarded as the baseline. Then, for different EV penetrations, the growth trend relative to the baseline is quantified in percentage terms. In addition, the number in brackets (∗) denotes the ACE or ATC growth rate between two adjacent EV penetrations.

In general, the increase of EV quantities incurs the increase for both objectives. When the EV number is up to 480, the minimized ATC increases by 9.59% compared to the baseline and the minimized ACE increase 11.37% accordingly. However, the variation of growth rate has implied that the objectives' change is not a proportional increase. The growth rate would gradually decrease to a certain level and stabilise, at which the total cost of integrating more EVs is decreasing and then stabilise. Explicitly, when the EV number is expanded to 300, the growth rates of ATC and AEC objectives stabilise at 1.3% and 1.8%, respectively.

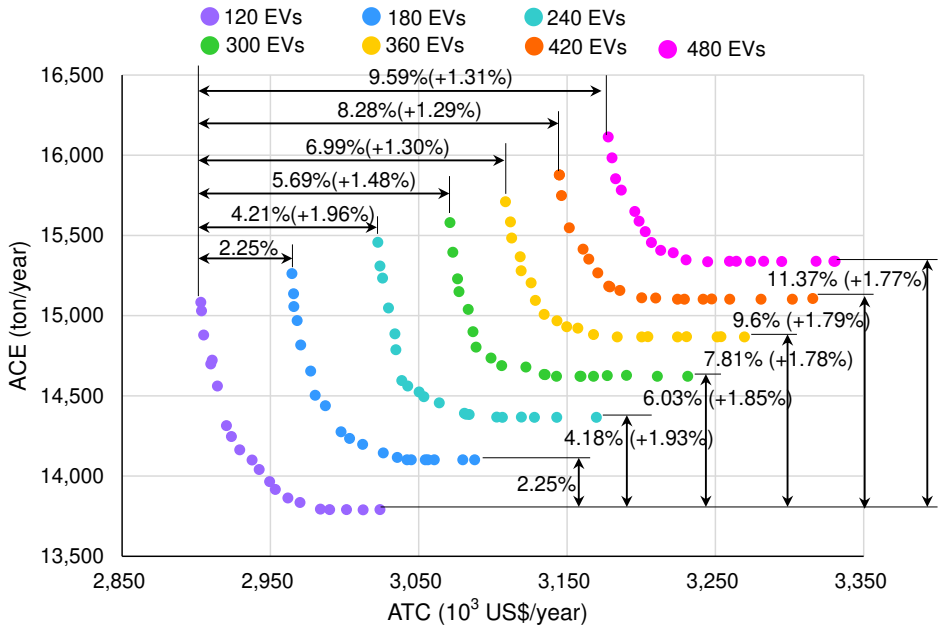

Fig. 15 Sensitivity analysis of EV penetration in Beijing commercial case.

5 Conclusion and the way forward

This study develops an optimisation model to quantify the benefits of embedding the vehicle-to-grid (V2G) into the integrated energy systems (IES) as a flexible energy storage. The system design, operation, and EV scheduling for the whole V2G-IES are optimised considering two trade-off objectives of cost and emissions. Through six cases with various climate conditions, energy prices, and demand patterns, the best V2G-IES demonstration cases and the V2G impact on the IES are analysed. The key findings are presented as follows.

(1) Enabling V2G with IES can indeed achieve the benefits on both cost and emission than the individual IES or EV operation mode.

(2) By optimal scheduling with IES, the V2G could act as a flexible energy storage which does not significantly the IES design and scheduling. The EVs charging schedule exhibits a large dependency on the real-time electricity price in summer and transition seasons while not in winter.

(3) Experimental uncertainty analysis indicates that the electricity purchasing price and natural gas price have significant impacts on the whole performance. Meanwhile, with the increasing EV into IES (up to 300 EVs), the total cost of integrating EVs is decreasing and finally stabilize to a certain level, at which the gain of the economic and environmental benefits stabilized at 1.3% and 1.8%, respectively.

In addition, future work could further explore the following two aspects: (1) The framework is extensive to consider the multiple agents' benefits such as capturing deeper interactions between EV users and the IES by investigating the faire V2G or G2V pricing strategies between IES and EVs users. (2) One modelling challenge lies in the EV user behaviours, which require more data processing methods, such as neural networks, support space vector, to approximate the EV travelling behaviour.

Acknowledgement

H.W. would like to thank for the support from the China Scholarship Council (Grant No. 201906030036).

Declaration of interest

There are no conflicts to declare.

Appendix

This appendix presents the technical parameters and the modelling constraints.

A1 Nomenclature and technical parameters

The definition of the parameters and variables are listed in Table A1~A3.

Table A1 Definition of indices

Abbreviations/Indices	Definitions
IES	Integrated energy system
V2G	Vehicle to grid
EV	Electric vehicles
CHP	Combined cooling heating and power
ATC	Annual total cost
ACE	Annual carbon emission
CAPEX	The installation cost of energy technologies
OPEX	The operation cost
FC	The fuel cost
MC	The maintenance cost
GC	The grid cost
DM	Diversity maximisation
NSGA-II	Nondominated sorting genetic algorithm II
SOC	State of charge for batteries
TOPSIS	Technique for order preference by similarity to an ideal solution
s	The technology type
h	Timeslot in the optimisation
clip	The clip operation
i	The number of EV

Table A2 Definition of the parameters in the optimisation

Parameters	Definitions	Values
CRF	Capital recovery factor	See [49]
r	The interest rate	5%

p	The service life	10
η^{CHP}	Efficiency of CHP during the gas to electricity	0.38
η_{CHP}^{E2H}	Conversion ratio of CHP between electricity and heating	1.1
η_{AC}^{H2C}	Efficiency of AC during the heating to cooling	1
η_{EC}^{E2C}	Efficiency of EC during the electricity to cooling	4
η^{HP}	Efficiency of heating pump	3.5
η^{Boiler}	Efficiency of boiler	0.85
C^{maint}	The maintenance cost	See [50]
C^{im}	The tariff for purchasing electricity	See **Fig. A1**
C^{ex}	The tariff for selling electricity	See **Fig. A1**
UC^{NG}	The unit cost of natural gas (Beijing, Shanghai, Xiamen)	See **Fig. A1**
ϑ^{grid}	Carbon emission factor of grid electricity (Beijing, Shanghai, Xiamen)	0.9419, 0.7921, 0.8042 (ton/kWh)
ϑ^{NG}	Carbon emission factor of natural gas (Beijing, Shanghai, Xiamen)	0.18 (ton/kWh)
T_{s}	The scheduling period	1 h
CAP^{EV}	The battery capacity	25 kWh
$E^{\max}$	The maximum of EV charging or discharging power	8 kW
E_{demand}	The electrical demand	See **Fig. 6**
Q_{demand}^{H}	The heating demand	See **Fig. 6**
Q_{demand}^{C}	The cooling demand	See **Fig. 6**
M_{upper}^{CHP}	The upper boundary of CHP capacity	10e3 kW
$M_{upper}^{\mathrm{grid}}$	The upper boundary of purchasing or selling electricity	10e3 kW
MOP	The minimum operational power factor of CHP	20%
RP	The ramping power constraint factor	50%

Table A3 Definition of variables.

Symbol	Definitions
Binary variables	
φ^{ex}	L(φ^{ex} >0)=1 if electricity is selling back to the grid
φ^{im}	L(φ^{im} >0)=1 if electricity is purchasing from the grid
ϕ^{CHP}	L(ϕ^{CHP} >0)=1 if the CHP is started
χ^{CHP}	L(χ^{CHP} >0)=1 if the CHP is only started once in a day
Variables	
CAP_s	The installed capacity for the technology *s*
UC^{cap}	The unit installation cost
E^{CHP}	Electrical energy generated by CHP

$P_{i,h}^{EV}$	The charging power of EV i at timeslot h
E^{im}	The amount of purchasing electricity
E^{ex}	The amount of selling electricity
E^{PV}	The electricity generated by photovoltaic
E^{HP}	The electricity consumed by heat pump
E^{EC}	The electricity consumed by electric chiller
E^{PV}	The electricity generated by photovoltaic
NG^{CHP}	The natural gas consumed by CHP
NG^{Boiler}	The natural gas consumed by boiler
Q^{Boiler}	Heating energy generated by boiler
Q^{HP}	Heating energy generated by heat pump
Q^{ACH}	Heating energy consumed by absorption chiller
Q^{ECC}	Cooling energy generated by electric chiller
Q^{ACC}	Cooling energy generated by absorption chiller
SOC_{cur}	The current SOC value of batteries
SOC_{ini}	The initial SOC value of batteries
X_{comm}	The probability distribution function of the charging duration in the commercial case
X_{comm}	The probability distribution function of the charging duration in the residential case
y_e	The objective value of solution in set E
α_E	The diversity degree
Δ_{ie}	The maximum error among all particles
ω_j	The positive weight factor
f^{norm}	The normalised objective value
$f^{ideal/nadir}$	The value of the “ideal” and “nadir” points
ED^{i+}	The Euclidean distance from the non-dominated solution to the ideal point.
ED^{i-}	The Euclidean distance from the non-dominated solution to the nadir point.
π	The *TOPSIS* index
ξ	The feasibility index for evaluating the feasible degree of charging pattern in cases

Note: L(·) denotes the logic function: if the content of function is positive, the value is 1; otherwise it is 0.

The energy prices including the purchasing price, feed-in tariff and gas price are illustrated in **Fig. A1**.

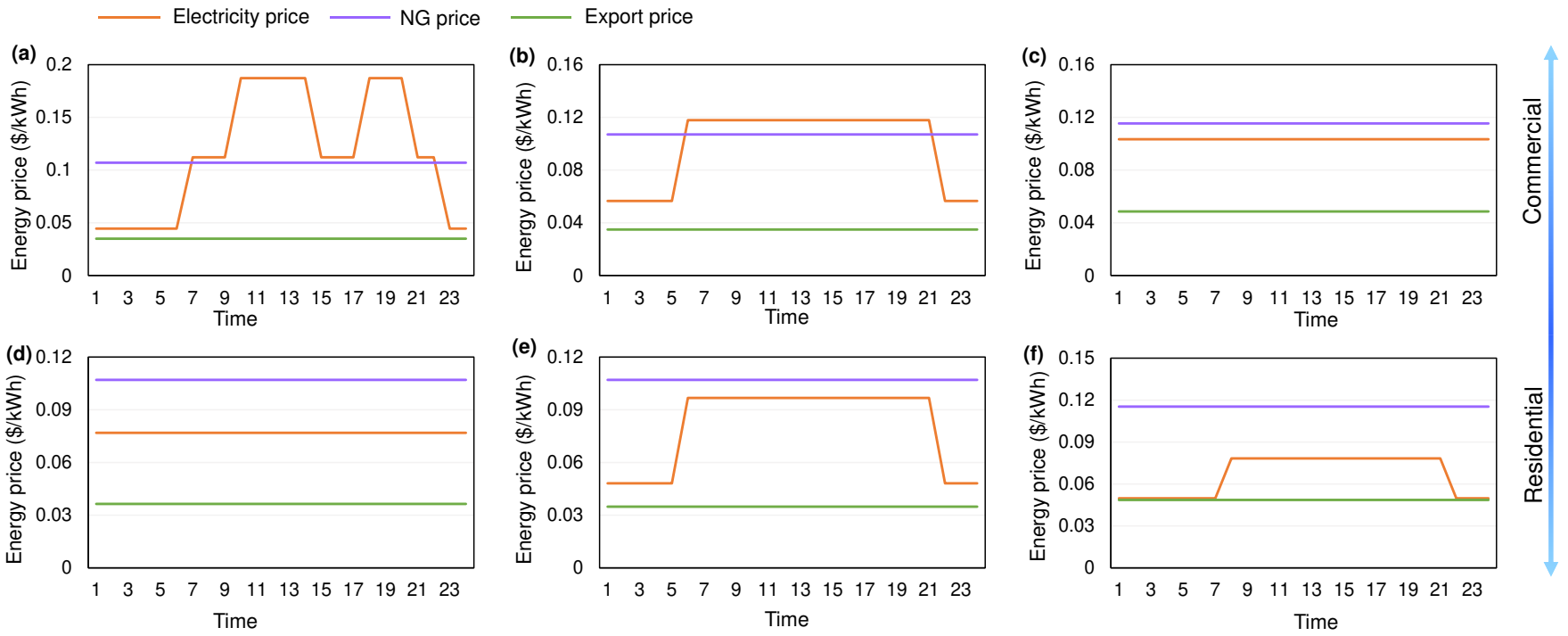

Fig. A1 Energy prices. (a) Beijing commercial; (b) Shanghai commercial; (c) Xiamen commercial; (d) Beijing residential; (e) Shanghai residential; (f) Xiamen residential.

Reference

[1] CEC. Communication from the Commission to the European Parliament, the Council, the European Economic and Social Committee and the Committee of the Regions: A Strategy for ICT R&D and Innovation in Europe: Raising the Game: Office for Official Publications of the European Communities, 2009.
[2] Pollitt H. Analysis: Going carbon neutral by 2060 'will make China richer'. Carbon Brief. 2020;24.
[3] Zhang S, Xiong R, Cao J. Battery durability and longevity based power management for plug-in hybrid electric vehicle with hybrid energy storage system. Applied energy. 2016;179:316-28.
[4] Alsharif A, Tan CW, Ayop R, Dobi A, Lau KY. A comprehensive review of energy management strategy in Vehicle-to-Grid technology integrated with renewable energy sources. Sustainable Energy Technologies and Assessments. 2021;47:101439.
[5] Wei H, Ai Q, Zhao W, Zhang Y. Modelling and experimental validation of an EV torque distribution strategy towards active safety and energy efficiency. Energy. 2021:121953.
[6] Soheyli S, Mayam MHS, Mehrjoo M. Modeling a novel CCHP system including solar and wind renewable energy resources and sizing by a CC-MOPSO algorithm. Applied Energy. 2016;184:375-95.
[7] Karmellos M, Mavrotas G. Multi-objective optimization and comparison framework for the design of Distributed Energy Systems. Energy Conversion and Management. 2019;180:473-95.
[8] Jing R, Wang M, Zhang Z, Wang X, Li N, Shah N, et al. Distributed or centralized? Designing district-level urban energy systems by a hierarchical approach considering demand uncertainties. Applied Energy. 2019;252:113424.
[9] Zhu X, Yang J, Pan X, Li G, Rao Y. Regional integrated energy system energy management in an industrial park considering energy stepped utilization. Energy. 2020;201:117589.
[10] Perera A, Nik VM, Chen D, Scartezzini J-L, Hong T. Quantifying the impacts of climate change and extreme climate events on energy systems. Nature Energy. 2020;5(2):150-9.
[11] Koltsaklis NE, Dagoumas AS. State-of-the-art generation expansion planning: A review. Applied energy. 2018;230:563-89.
[12] Rabiee A, Mohseni-Bonab SM. Maximizing hosting capacity of renewable energy sources in distribution networks: A multi-objective and scenario-based approach. Energy. 2017;120:417-30.
[13] Yang H, Xiong T, Qiu J, Qiu D, Dong ZY. Optimal operation of DES/CCHP based regional multi-energy prosumer with demand response. Applied Energy. 2016;167:353-65.

[14] Wang M, Yu H, Jing R, Liu H, Chen P, Li C. Combined multi-objective optimization and robustness analysis framework for building integrated energy system under uncertainty. Energy Conversion and Management. 2020;208:112589.
[15] Qin X, Sun H, Shen X, Guo Y, Guo Q, Xia T. A generalized quasi-dynamic model for electric-heat coupling integrated energy system with distributed energy resources. Applied Energy. 2019;251:113270.
[16] Perera A, Javanroodi K, Nik VM. Climate resilient interconnected infrastructure: Co-optimization of energy systems and urban morphology. Applied Energy. 2021;285:116430.
[17] Lv J, Li Y, Shan B, Jin S, Suo C. Planning energy-water nexus system under multiple uncertainties–A case study of Hebei province. Applied Energy. 2018;229:389-403.
[18] Wang F, Xu J, Liu L, Yin G, Wang J, Yan J. Optimal design and operation of hybrid renewable energy system for drinking water treatment. Energy. 2021;219:119673.
[19] Pfeifer A, Herc L, Bjelić IB, Duić N. Flexibility index and decreasing the costs in energy systems with high share of renewable energy. Energy Conversion and Management. 2021;240:114258.
[20] Jin M, Feng W, Marnay C, Spanos C. Microgrid to enable optimal distributed energy retail and end-user demand response. Applied Energy. 2018;210:1321-35.
[21] Jing R, Hastings A, Guo M. Sustainable design of urban rooftop food-energy-land nexus. Iscience. 2020;23(11):101743.
[22] Geske J, Schumann D. Willing to participate in vehicle-to-grid (V2G)? Why not! Energy Policy. 2018;120:392-401.
[23] Farahani HF, Rabiee A, Khalili M. Plug-in electric vehicles as a harmonic compensator into microgrids. Journal of Cleaner Production. 2017;159:388-96.
[24] Dallinger D, Gerda S, Wietschel M. Integration of intermittent renewable power supply using grid-connected vehicles–A 2030 case study for California and Germany. Applied Energy. 2013;104:666-82.
[25] Das R, Wang Y, Putrus G, Kotter R, Marzband M, Herteleer B, et al. Multi-objective techno-economic-environmental optimisation of electric vehicle for energy services. Applied Energy. 2020;257:113965.
[26] Zhang C, Greenblatt JB, MacDougall P, Saxena S, Prabhakar AJ. Quantifying the benefits of electric vehicles on the future electricity grid in the midwestern United States. Applied Energy. 2020;270:115174.
[27] Jing R, Wang J, Shah N, Guo M. Emerging supply chain of utilising electrical vehicle retired batteries in distributed energy systems. Advances in Applied Energy. 2021;1:100002.
[28] Ahmad MS, Sivasubramani S. Optimal number of electric vehicles for existing networks considering economic and emission dispatch. IEEE Transactions on Industrial Informatics.

2018;15(4):1926-35.
[29] Tran M-K, DaCosta A, Mevawalla A, Panchal S, Fowler M. Comparative Study of Equivalent Circuit Models Performance in Four Common Lithium-Ion Batteries: LFP, NMC, LMO, NCA. Batteries. 2021;7(3):51.
[30] Duan J, Zhao J, Li X, Panchal S, Yuan J, Fraser R, et al. Modeling and Analysis of Heat Dissipation for Liquid Cooling Lithium-Ion Batteries. Energies. 2021;14(14):4187.
[31] Shi R, Li S, Zhang P, Lee KY. Integration of renewable energy sources and electric vehicles in V2G network with adjustable robust optimization. Renewable Energy. 2020;153:1067-80.
[32] Fathabadi H. Utilization of electric vehicles and renewable energy sources used as distributed generators for improving characteristics of electric power distribution systems. Energy. 2015;90:1100-10.
[33] Sedighizadeh M, Esmaili M, Mohammadkhani N. Stochastic multi-objective energy management in residential microgrids with combined cooling, heating, and power units considering battery energy storage systems and plug-in hybrid electric vehicles. Journal of Cleaner Production. 2018;195:301-17.
[34] Akhoundzadeh MH, Panchal S, Samadani E, Raahemifar K, Fowler M, Fraser R. Investigation and simulation of electric train utilizing hydrogen fuel cell and lithium-ion battery. Sustainable Energy Technologies and Assessments. 2021;46:101234.
[35] Wolinetz M, Axsen J, Peters J, Crawford C. Simulating the value of electric-vehicle–grid integration using a behaviourally realistic model. Nature Energy. 2018;3(2):132-9.
[36] Qian K, Zhou C, Allan M, Yuan Y. Modeling of load demand due to EV battery charging in distribution systems. IEEE transactions on power systems. 2010;26(2):802-10.
[37] Zhou Y, Yau DK, You P, Cheng P. Optimal-cost scheduling of electrical vehicle charging under uncertainty. IEEE Transactions on Smart Grid. 2017;9(5):4547-54.
[38] Mu Y, Wu J, Jenkins N, Jia H, Wang C. A spatial–temporal model for grid impact analysis of plug-in electric vehicles. Applied Energy. 2014;114:456-65.
[39] Lin H, Wang Q, Wang Y, Liu Y, Huang N, Wennersten R, et al. A multi-agent based optimization architecture for energy hub operation. Energy Procedia. 2017;142:2158-64.
[40] Zakariazadeh A, Jadid S, Siano P. Multi-objective scheduling of electric vehicles in smart distribution system. Energy Conversion and Management. 2014;79:43-53.
[41] MEEPC. Baseline emission factors of China's regional power grid for emission reduction projects in 2019. 2019.
[42] Hoke A, Brissette A, Smith K, Pratt A, Maksimovic D. Accounting for lithium-ion battery degradation in electric vehicle charging optimization. IEEE Journal of Emerging and Selected Topics in Power Electronics. 2014;2(3):691-700.

[43] U.S. Department of Transportation FHA. National Household Travel Survey. 2017.
[44] Wei H, Zhang N, Liang J, Ai Q, Zhao W, Huang T, et al. Deep reinforcement learning based direct torque control strategy for distributed drive electric vehicles considering active safety and energy saving performance. Energy. 2022;238:121725.
[45] Deb K, Pratap A, Agarwal S, Meyarivan T. A fast and elitist multiobjective genetic algorithm: NSGA-II. IEEE transactions on evolutionary computation. 2002;6(2):182-97.
[46] Kang Q, Feng S, Zhou M, Ammari AC, Sedraoui K. Optimal load scheduling of plug-in hybrid electric vehicles via weight-aggregation multi-objective evolutionary algorithms. IEEE Transactions on Intelligent Transportation Systems. 2017;18(9):2557-68.
[47] Wei H, Liang J, Li C, Zhang Y. Real-Time Locally Optimal Schedule for Electric Vehicle Load via Diversity-Maximization NSGA-II. Journal of Modern Power Systems and Clean Energy. 2020.
[48] Feng Y, Hung T, Greg K, Zhang Y, Li B, Yang J. Thermoeconomic comparison between pure and mixture working fluids of organic Rankine cycles (ORCs) for low temperature waste heat recovery. Energy Conversion and Management. 2015;106:859-72.
[49] Wang M, Yu H, Lin X, Jing R, He F, Li C. Comparing stochastic programming with posteriori approach for multi-objective optimization of distributed energy systems under uncertainty. Energy. 2020;210:118571.
[50] Jing R, Zhu X, Zhu Z, Wang W, Meng C, Shah N, et al. A multi-objective optimization and multi-criteria evaluation integrated framework for distributed energy system optimal planning. Energy Conversion and Management. 2018;166:445-62.